Forward Differential Cross Sections for the Reaction $p+p \rightarrow d+\pi^+$ in the Range 3.4–12.3 GeV/c†

L. L. ANDERSON, M. S. DIXIT, H. J. EVANS, K. A. KLARE, D. A. LARSON, AND M. V. SHERBROOK
The Enrico Fermi Institute, The University of Chicago, Chicago, Illinois 60637

AND

R. L. MARTIN
Argonne National Laboratory, Argonne, Illinois 60439

AND

D. KESSLER
Carleton University, Ottawa, Canada

AND

D. E. NAGLE AND H. A. THIESSEN
University of California, Los Alamos Scientific Laboratory, Los Alamos, New Mexico 87544

AND

C. K. HARGROVE AND E. P. HINCKS*
National Research Council of Canada, Ottawa, Canada

AND

S. FUKUI
Nagoya University, Nagoya, Japan

(Received 20 November 1970)

A missing-mass spectrometer, employing optical spark chambers with automatic vidicon readout, was used to measure the forward differential cross section ($\cos\theta_{\text{c.m.}} \approx 0.995$) for the reaction $p+p \rightarrow d+\pi^+$ at closely spaced settings of the incident proton momentum in the range $p_0 = 3.4$–12.3 GeV/c. The deuterons from the reaction were identified by time of flight, and their momentum and angle of emission measured by a reconstruction of the spark-chamber tracks. Since the incoming proton momentum was accurately known, the missing mass associated with deuteron production could be deduced. The reaction $p+p \rightarrow d+\pi^+$ was identified by the appearance of a distinct peak corresponding to the pion mass in a missing-mass plot. The data confirm the existence of a prominent peak in the forward cross section at $E_{\text{c.m.}} = 3.0$ GeV and show a hitherto unreported shoulder at $E_{\text{c.m.}} = 3.7$ GeV. This structure, along with the well-known sharp maximum at $E_{\text{c.m.}} = 2.2$ GeV, may be understood on the basis of a one-pion-exchange model as reflecting the behavior of the $T = \frac{3}{2}$ isobars in pion-nucleon scattering. Above $E_{\text{c.m.}} = 3.9$ GeV, the forward differential cross section decreases monotonically as the -2.5 power of s, the square of the total c.m. energy. This feature also reflects the behavior of the πp scattering cross section. The structureless upper-energy region can also be accommodated within the framework of Regge theory. The cross section $d\sigma/du$ extrapolated to $u=0$ varies as the -3.2 power of s, midway between that expected for the N_α and N_γ trajectories.

I. INTRODUCTION

IN the course of a general survey of bosons produced in high-energy pp collisions, an extensive set of forward differential cross sections was measured for the reaction

$$p+p \rightarrow d+\pi^+ \qquad (1)$$

over the range of incident momenta 3.4–12.3 GeV/c. In this paper we describe this aspect of the work and present a detailed description of the apparatus and the measurements, together with what can be said of the significance of the results. A brief Letter has already been published.[1]

The general method of our work was to use the observation of the production of a deuteron as a device for determining the fate of the two nucleons of the initial state. Since the initial two-proton state has isospin $T=1$ and the deuteron has $T=0$, whatever else is produced must have a total isospin $T=1$ and have baryon number $B=0$. The pion is the simplest object with these quantum numbers and turned out to be easy to identify by the missing-mass (MM) technique. By knowing the momentum and direction of the incoming proton and by measuring precisely the momentum and angle of the emergent deuteron, we could deduce the MM of whatever else was produced. Single-pion production could be identified because of the appearance of a distinct peak, generally with low background, at the pion-mass position in a MM plot.

Reaction (1) has particular importance in high-energy physics because it is one of the few two-body reactions which is experimentally accessible in direct, inverse, as well as in the crossed channels. It thus

† Research supported by the National Science Foundation, the U. S. Atomic Energy Commission, and the National Research Council of Canada. Submitted by M. V. Sherbrook to the Department of Physics, The University of Chicago, in partial fulfillment of the requirements for the Ph.D. degree.

* Also at Carleton University, Ottawa, Canada.

[1] H. L. Anderson, M. S. Dixit, H. J. Evans, K. A. Klare, D. A. Larson, M. V. Sherbrook, R. L. Martin, K. W. Edwards, D. Kessler, D. E. Nagle, H. A. Thiessen, C. K. Hargrove, E. P. Hincks, and S. Fukui, Phys. Rev. Letters **21**, 853 (1968).

provides an opportunity to test the theorems that govern the relationships among these channels. Early measurements at low energies[2] used the comparison of the direct and inverse channels and the principle of detailed balance to establish that the spin of the pion is zero.

When we began our study very few measurements had been made above 3.6 GeV/c incident proton momentum. On the other hand, a relatively rich body of literature dealt with the measurements and their interpretation below this. A reasonably satisfactory account of the very low-energy behavior had been provided by the phenomenological analysis of Rosenfeld[3] and of Gell-Mann and Watson.[4] However, this was suitable only when few angular-momentum states were involved. The resonant behavior that appeared at 660 MeV proton energy was analyzed by Mandelstam[5] in terms of what we might today refer to as a direct-channel resonance in which the pion and one of the nucleons are in a $(\frac{3}{2}, \frac{3}{2})$ isobaric state, and this in turn is in an S-state interaction with the second nucleon. Such a state, with angular momentum $J=2$ fed from a $^1D_2$ diproton initial state, gives a plausible if not entirely satisfactory account of the peak at 2.17 GeV c.m. energy.

The Mandelstam approach owes its success to the small number of angular momentum states which can contribute in the low-energy region. More detailed measurements of the reaction in this energy region recently obtained by Richard-Serre[6] have shown the complications that enter due to the influence of higher angular-momentum states.

When measurements at somewhat higher energy were carried out,[7–11] the popular approach was to analyze the data in terms of one-pion-exchange (OPE) and one-nucleon-exchange (ONE) models. In the work of Heinz *et al.*[9] in the energy region between 1 and 2.8 GeV, neither model proved quantitatively satisfactory, but the qualitative behavior of the ONE model led these authors to conclude that the ONE process could conceivably be the dominant mechanism, and that with suitable refinements, the model could give better quantitative agreement with the experiment.

Such a conclusion seems unjustified in view of the marked resonant behavior which was evident just below 1 GeV, since ONE provides no mechanism for such behavior. It is difficult to see how refinements in the model alone could help resolve this situation. On the other hand, it was pointed out to us by Silbar,[12] on the basis of a OPE model, that a rich structure could be expected at higher energies because of the influence of the resonances that show up in πp scattering.

Here, and more generally in strong-interaction physics, with only primitive theoretical tools available there are a variety of possible models which are in some degree plausibile from seemingly quite different points of view. It is not even clear that it is a matter of choice among them. The duality argument[13] suggests that different models may represent equivalent ways of describing the same thing. To help clarify the situation, there is a need for more detailed data over a wider range of the observable parameters. We present here a substantial addition to the data available in the range 3.4–12.3 GeV/c incident momentum, where previously only a few measurements were available.

The forward differential cross section for reaction (1) was measured in this experiment at 29 settings of the incident proton laboratory momentum in the range $p_0=3.4$–12.3 GeV/c. The deuteron spectrometer, employing optical spark chambers with an automatic vidicon readout, was used to determine the deuteron momentum and angle of emission. The laboratory production angle of the deuterons was held fixed at 5° with respect to the incident proton beam. We detected the deuterons emitted backward in the c.m. system, but, due to the symmetry of the initial state of reaction (1), no distinction need be made between positive and negative values of $\cos\theta_{\text{c.m.}}$. The $\cos\theta_{\text{c.m.}}$ was nearly constant, varying from 0.9928 at the lowest incident momentum to 0.9985 at the highest. The laboratory momentum of the backward deuterons covered the range $p_d=1.14$–1.34 GeV/c. The transverse momentum was small, varying from 0.099 to 0.116 GeV/c. The total c.m. energy covered the range $E_{\text{c.m.}}=2.9-5.0$ GeV.

II. EXPERIMENTAL TECHNIQUE

In the MM method used in this experiment, only the deuteron was detected. The presence of the pion was inferred from energy-momentum conservation using the known momentum of the incoming proton and the measured momentum and angle of the emergent deuteron. Taking p_1 and p_2 to be the four-momenta of the incident and target protons, respectively, energy-momentum conservation may be written $p_1+p_2=p_3+p_x$, where p_3 is the four-momentum of the deuteron

[2] R. Durbin, H. Loar, and J. Steinberger, Phys. Rev. **83**, 646 (1951); D. L. Clark, A. Roberts, and R. Wilson, *ibid.* **83**, 649 (1951); W. F. Cartwright, C. Richman, M. N. Whitehead, and H. A. Wilcox, *ibid.* **91**, 677 (1953).

[3] A. H. Rosenfeld, Phys. Rev. **96**, 139 (1954).

[4] M. Gell-Mann and K. M. Watson, Ann. Rev. Nucl. Sci. **4**, 219 (1954).

[5] S. Mandelstam, Proc. Roy. Soc. (London) **A244**, 491 (1958).

[6] C. Richard-Serre, CERN Report No. 68-40 (unpublished).

[7] K. R. Chapman, T. W. Jones, Q. H. Khan, J. S. C. McKee, H. B. Van Der Raay, and Y. Tanimura, Phys. Letters **11**, 253 (1964).

[8] D. Dekkers, B. Jordan, R. Mermod, C. C. Ting, G. Weber, T. R. Willitts, K. Winter, X. De Bouard, and M. Vivargent, Phys. Letters **11**, 161 (1964).

[9] R. M. Heinz, O. E. Overseth, D. E. Pellett, and M. L. Perl, Phys. Rev. **167**, 1232 (1968).

[10] F. Turkot, G. B. Collins, and T. Fujii, Phys. Rev. Letters **11**, 474 (1963).

[11] G. Cocconi, E. Lillethun, J. P. Scanlon, C. A. Ståhlbrandt, C. C. Ting, J. Walters, and A. M. Wetherell, Phys. Letters **7**, 222 (1963).

[12] R. R. Silbar (private communication).

[13] C. Schmid, Phys. Rev. Letters **20**, 689 (1968).

and p_x the four-momentum of whatever else is produced. Solving for the Lorentz-invariant scalar p_x^2, we obtain the desired quantity, the missing mass squared (MM^2). Reaction (1) is identified by the presence of a peak corresponding to the pion mass in a plot of MM^2.

The deuterons, momentum-analyzed within the spectrometer, were separated from the much more numerous protons and pions by a time-of-flight (TOF) technique. Deuterons, so identified, triggered the spark chambers and vidicon system. The images of the spark-chamber tracks in the vidicons were digitized and recorded on magnetic tape. From the record of the spark-chamber track locations, the deuteron trajectory through the spectrometer was reconstructed and its momentum and angle of emission calculated. Figure 1 shows the kinematical relationship between the deuteron laboratory momentum and angle for reaction (1) for the minimum and maximum incident proton momenta observed in this experiment. The region studied corresponds to deuterons emitted backward in the c.m. system. We choose to observe the backward deuterons because their smaller laboratory momentum simplified the TOF measurement. In addition, the deuteron laboratory momentum is nearly independent of angle near 5°, which in turn implies that the MM is nearly angle independent.

A. Experimental Layout

The MM spectrometer was set up in the external proton beam (EPB) of the zero-gradient synchrotron (ZGS) at the Argonne National Laboratory. A diagram of the layout is shown in Fig. 2. The liquid-hydrogen target was located immediately outside the shielding wall of the ring building. The hydrogen flask was a 7.62-cm diameter cylinder with vertical axis, constructed of 76-μ Kapton and wrapped in several layers of 6.4-μ aluminized Mylar superinsulation. In order to minimize the flux of nonhydrogen deuterons in the spectrometer, the flask was suspended by its filling lines

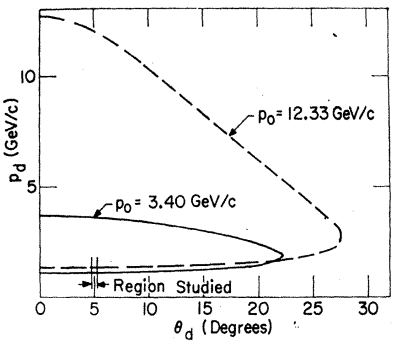

FIG. 1. Kinematics diagram for the reaction $p+p \rightarrow d+\pi^+$ expressed in terms of the deuteron laboratory momentum p_d and angle θ_d. The solid curve corresponds to the minimum incident proton momentum observed $p_0=3.4$ GeV/c and the dashed curve to the maximum $p_0=12.3$ GeV/c. The region studied corresponds to deuterons moving backward in the c.m. system.

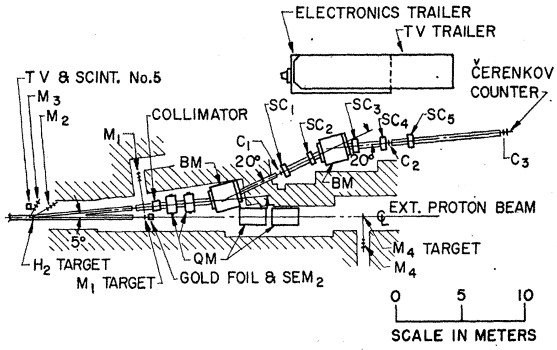

FIG. 2. Experimental arrangement.

in a continuous Y-shaped vacuum pipe, which extended approximately 6 m upstream into the ring building and 7 m downstream along both the EPB and the secondary 5° line of this experiment.

The laboratory solid-angle acceptance of the spectrometer (2.08×10^{-4} sr) was defined by a 61-cm lead collimator (9.52 cm width$\times$19.7 cm height) located 9.50 m from the hydrogen target. After passing through the collimator, the secondary beam entered the spectrometer, which was set to accept positively charged particles. The spectrometer consisted of a quadrupole pair, two bending magnets in reverse-bend configuration, five spark chambers with vidicon readout (SC_1, SC_2, SC_3, SC_4, and SC_5), three TOF counters (C_1, C_2, and C_3), and a glycerol threshold Čerenkov counter. The first bending magnet served to bend the particles 20° in a direction away from the EPB and out of the proton tunnel. The second bending magnet served as the momentum analyzer. It was arranged to bend the particles 20° in a direction counter to the bend of the first magnet and parallel to their initial direction. A secondary emission monitor (SEM_2) and four proton-beam monitors (M_1, M_2, M_3, and M_4) were located along the proton line as shown in Fig. 2.

In order to minimize multiple Coulomb scattering of the deuterons, a helium atmosphere was maintained all along the spectrometer arm, from the end of the vacuum transport within the proton tunnel to counter C_3, with air gaps introduced only at the TOF counters. The spark chambers, themselves, were maintained in a helium atmosphere. The helium transport system consisted of aluminum pipes through the bending magnets and shielding wall with polyethylene bags connected directly to the spark-chamber housing in the intervening spaces.

The electronics trailer was centrally located with the television trailer mounted above it on a stand in order to conserve floor space in the experimental area.

B. Proton Beam and Monitors

The EPB momentum was varied from 3.4 to 12.3 GeV/c by using the "front porch" feature of the ZGS. The internal proton beam of about 2×10^{12} protons/

pulse was accelerated up to the desired energy, a portion extracted while maintaining the ZGS field constant, and the remainder accelerated to full energy for other use. Spills were from 300 to 500 msec in length with a repetition period that varied from 2.6 to 3.5 sec. The extracted beam intensity was usually limited to about 10^{11} protons/pulse so as not to exceed about 1.5×10^5 particles/pulse in the first spark chamber SC_1. The beam had a momentum spread of about ±10 MeV/c and an absolute energy calibration correct to about $\pm\frac{1}{2}\%$.

The determination of the differential cross section for reaction (1) required a knowledge of the absolute number of protons that traversed the hydrogen target during a particular measurement. However, the proton-beam intensity could not be measured directly by conventional counting techniques because of the high rate (10^{11}–10^{12} protons/sec). Therefore, the protons were counted indirectly by monitor M_1 which observed the secondary spray when the EPB struck a 6.4-mm-thick Plexiglas target located on a stand 7.6 m downstream of the hydrogen target and immediately upstream of the SEM_2 stand (see Fig. 2). Monitor M_1 (as well as M_2, M_3, and M_4) consisted of a linear array of three identical counters in coincidence. The M_1 counts were in turn related to the absolute number of protons in the EPB by gold-foil activation, and consisted of counting the α branch of Tb^{149} produced in gold by proton bombardment. The techniques used were established for the EPB of the ZGS and have been discussed in detail by Steinberg *et al.*[14] We shall return to this subject later.

The external proton line was tuned using a diagnostic system of television cameras and monitor telescopes. The beam upstream of our target could be observed via television which viewed gridded plastic scintillators located along the transport system. These scintillators could be flipped out of the beam when not in use. As shown in Fig. 2, M_2 viewed the hydrogen target. It aided in centering the beam on the target, as well as giving a continuous check on the status of the target. Monitor M_3 viewed a section of the vacuum pipe immediately upstream of the hydrogen target. Deviations of M_3 from its nominal value were a good indication that the beam was striking the transport system upstream. The SEM_2 was used for checking the instantaneous beam intensity as well as the transport efficiency from the ZGS ring by comparing it with another secondary emission monitor, located just outside the ring. Monitor M_4 viewed a Plexiglas target (15.2 cm$\times$15.2 cm$\times$4.0 mm) mounted on a motorized table top and located approximately 24 m downstream of the hydrogen target. It was used for checking the beam centering for other users downstream.

Preliminary EPB transport solutions were obtained by computer and the final operating conditions by empirical tuning. Acceptable conditions were reached by centering the beam on the TV scintillators, maximizing M_2 while minimizing M_3, centering the beam with M_4, and checking the spectrometer rates with an empty target. A Polaroid film was exposed at the M_1 target to check beam position and angular divergence. The cross section and angular divergence of the EPB at the hydrogen target often represented a compromise between the desired conditions and the requirements of the downstream users. The cross section was usually less than about 3 cm^2 and the angular divergence did not exceed ±5 mrad in either the horizontal or vertical plane. The beam was close to a focus at the hydrogen target.

C. Spectrometer

The magnetic elements of the spectrometer consisted of a quadrupole pair and two bending magnets. The quadrupoles (ZGS designation QM-104) had a 25.7 cm bore, 49.3 cm effective length, and a minimum focal length of 76 cm at 1 GeV/c. The first bending magnet (ZGS designation BM-105), located just inside the EPB shielding, had a 38.6-cm horizontal by 15.2-cm vertical gap and a maximum $\int\mathbf{B}\cdot d\mathbf{l}$ of 3400 kG cm. The momentum measuring magnet (ZGS designation BM-109) had a 61.0-cm horizontal by 20.3-cm vertical gap and a maximum $\int\mathbf{B}\cdot d\mathbf{l}$ of 3500 kG cm. The effective length of the bending magnets was known to about 0.1%.

The 5° emission angle of the deuterons was chosen in order to be as close as possible to 0° without going into the EPB with a magnet. The first bending magnet in the spectrometer was necessary because of the small production angle being observed and the need to get the secondary beam away from the EPB and out of the proton tunnel. The spectrometer bending angle was chosen at 20°. This provided sufficient working space for the spectrometer, an adequate momentum measuring resolution of $\pm\frac{1}{3}\%$, an acceptable momentum bite of $\pm4\%$, and a maximum central momentum of 3.0 GeV/c.

The magnets were arranged in the reverse-bend configuration in order to compensate for the angular dispersion introduced by the first bending magnet. The quadrupoles helped provide a relatively large solid angle. By choosing the horizontal focus near counter C_3, the displacement from the optical axis after the second bending magnet did not depend strongly on the initial deuteron angle. At C_3 the displacement was independent of the initial deuteron angle and depended primarily on the deuteron momentum, at least for a point source. The spatial dispersion at C_3 was 3 mm per MeV/c at 1 GeV/c. The vertical focus was chosen near the center of the second bending magnet in order to maximize the solid angle.

Figure 3 shows the calculated spectrometer acceptance for central spectrometer momentum $p_s=1.14$

[14] E. P. Steinberg, A. F. Stehney, C. Stearns, and I. Spaletto, Nucl. Phys. **A113**, 265 (1968).

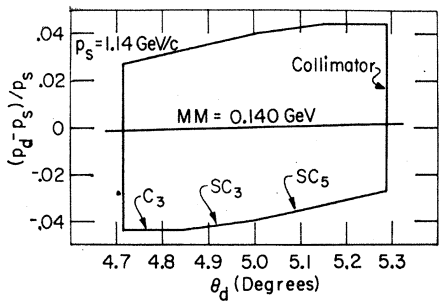

FIG. 3. Acceptance window for the spectrometer as calculated by the matrix technique for incident proton momentum $p_0=3.4$ GeV/c and spectrometer setting $p_s=1.14$ GeV/c. Shown in the window is the kinematic line for the pion missing mass MM = 0.140 GeV. The momentum acceptance is limited by time-of-flight counter C_3 and spark chambers SC_3 and SC_5. The angular acceptance is limited by the collimator.

GeV/c. Included in the acceptance window is the kinematic line for reaction (1) at $p_0=3.4$ BeV/c. Also indicated are the apertures which limit the acceptance. These are sharp, the target being idealized as a point source. The angular acceptance of $\pm 0.3°$ (± 5 mrad) at the central momentum was determined by the collimator. If counter C_3 had been the only aperture limiting the momentum bite, the acceptance would have been rectangular. However, as indicated in Fig. 3, spark chambers SC_3 and SC_5 cut into the acceptance somewhat, thus limiting the momentum bite to about $\pm 2.7\%$ while still accepting the full angular spread of ± 5 mrad at the central momentum.

The actual acceptance of the spectrometer does not have the sharp outline indicated in Fig. 3, but has rounded edges because of the finite target size, finite vertical aperture, and the multiple Coulomb scattering of the deuterons. A Monte Carlo program computed this acceptance by randomly choosing the three coordinates of the vertex in the target, the deuteron momentum, and the angle of emission of the deuteron. It traced the deuteron through the spectrometer, taking into account energy loss and multiple scattering. Figure 4 shows the calculated spectrometer efficiency curves for deuterons which passed through the collimator and ultimately reached counter C_3 versus the quantity $(p_d-p_s)/p_s$ for spectrometer momenta of 1.14 and 1.34 GeV/c. Also shown in Fig. 4 are the points corresponding to an experimental measurement of the spectrometer efficiency, discussed below. The Monte Carlo calculation shows that the acceptance is flat in the region $\pm 1.5\%$ about the central momentum. All deuterons that passed through the collimator within this momentum range were accepted by the spectrometer, except for a small loss from multiple scattering. From the results of the Monte Carlo calculation, the scattering loss at 1.14 and 1.34 GeV/c was found to be 4.7 and 1.3%, respectively. The program was run at 1.2, 1.4, and 1.7 GeV/c, and the scattering loss at other central momenta was determined by quadratic interpolation.

At an incident proton momentum of 4.0 GeV/c, the spectrometer acceptance was measured using deuterons from reaction (1). This was accomplished by moving the spectrometer window across the pion-mass line and observing the drop in yield from reaction (1) as the mass line moved out of the window. At $p_0=4.0$ GeV/c, the deuterons from reaction (1) have a momentum of 1.18 GeV/c. Therefore, the spectrometer was swept across the pion-mass line from 1.13 to 1.24 GeV/c in steps of 0.01 GeV/c. The resulting measurements, normalized to the yield at $p_s=1.18$ GeV/c and adjusted to include the multiple Coulomb scattering loss, are plotted in Fig. 4. They are in good agreement with the acceptance calculated by the Monte Carlo program.

D. Counters and Electronics

The deuterons were identified by selecting their momenta in a specified range (approximately $\pm 4\%$ of the central spectrometer momentum) and then measuring their TOF's. For the momenta of interest in this experiment ($p_d=1.14$–1.34 GeV/c), deuterons have a velocity $\beta \approx 0.5$, while the protons have $\beta \approx 0.75$ and the pions $\beta \approx 1$. We were able to distinguish the deuterons easily from the much more numerous protons and pions with a reasonable flight path.

Since the backward deuterons from reaction (1) in the vicinity of 5° in the laboratory are nearly monoenergetic for a fixed incident proton energy, it was possible to identify the deuterons from reaction (1) using TOF alone. With the spectrometer set on the deuteron momentum for reaction (1), the TOF distribution for deuterons appeared as a sharp peak centered on a broad background of nonhydrogen deuterons.

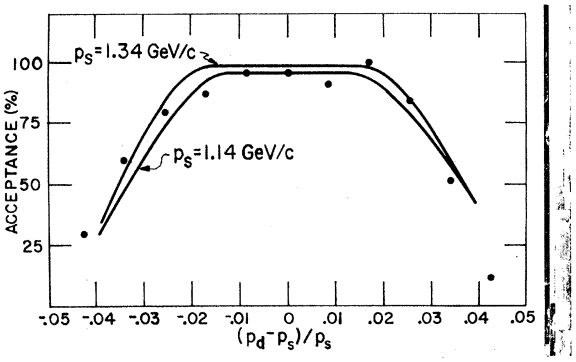

FIG. 4. Spectrometer efficiency as calculated by a Monte Carlo program which randomly chose the events and traced them through the spectrometer for $p_s=1.14$ and 1.34 GeV/c. The fact that the efficiency curves do not reach 100% at the central spectrometer setting is a measure of the losses from multiple Coulomb scattering. The points are an experimental measurement of the spectrometer efficiency using deuterons from the reaction $p+p \rightarrow d+\pi^+$ with momentum $p_d=1.18$ GeV/c. The spectrometer window was swept across the pion-mass line and the deuteron yield measured as a function of the spectrometer setting p_s. The experimental points are normalized to the yield at the central value $p_s=1.18$ GeV/c and adjusted to reflect the loss from multiple scattering. The size of the experimental points indicate the statistical error.

This technique provided a measurement of the differential cross section without reference to the spark chambers, as will be discussed below.

In counters employing large scintillators, the position variation of the event within the scintillator and the subsequent transit-time spread of the photons to the photomultiplier can contribute significantly to the timing uncertainty of the event. For the size of the counters used in this experiment, the vertical-position spread could have introduced an uncertainty of about ± 1.5 nsec. This uncertainty can be cut in half by viewing the scintillator at the upper and lower edges and merely accepting the first photomultiplier to fire. We have, however, made use of the fact that the sum of the transit times for the direct light from the event to opposite edges of the scintillator is a constant and independent of position. If the TOF between the same pair of counters is measured twice, employing the upper tubes for one measurement and the lower tubes for the other measurement, and if the two measurements are added, the vertical position spread can be essentially canceled.

Time-of-flight counters C_1 and C_2 each consisted of five 3.2-mm-thick by 5.7-cm-wide plastic scintillators viewed at both the upper and lower end by RCA 8575 photomultipliers. Each counter required six tubes. The scintillators and light guides were arranged as shown in Fig. 5, thus giving hodoscope capabilities in the horizontal direction to the counters, as well as improved time resolution. Counters C_1 and C_2, along with their associated local logics, were identical except for the lengths of scintillator, which were 17.8 and 27.9 cm, respectively. Counter C_3 consisted of a single sheet of plastic scintillator (27.9 cm$\times$27.9 cm$\times$64 mm) which was viewed at both the upper end and the lower end by an RCA 8575 photomultiplier.

In order to minimize the cable length through which the raw photomultiplier tube pulses were required to travel, a system of local logics was placed within close proximity (1.5–3 m) to each of the TOF counters. The electronic circuitry at both the local logics and the main logics in the electronics trailer largely used M100 modules manufactured by Edgerton, Germeshausen and Grier, Inc. (EGG). Figure 6 gives a block diagram of the local logics for either C_1 or C_2. It is apparent that five twofold coincidences were required per counter in order to define the scintillator through which the particle passed. These hodoscope coincidences were formed, apart from the TOF circuitry, at the local logics, eventually strobed by a deuteron event, and recorded on magnetic tape to be used in the analysis for cross checking the spark-chamber retrace. As indicated in Fig. 6, all upper tubes were ORed together, and all lower tubes were ORed together. The input pulses at the OR circuits were timed together to within about 1/10 nsec using General Radio constant-impedance trombones and time-to-amplitude converters

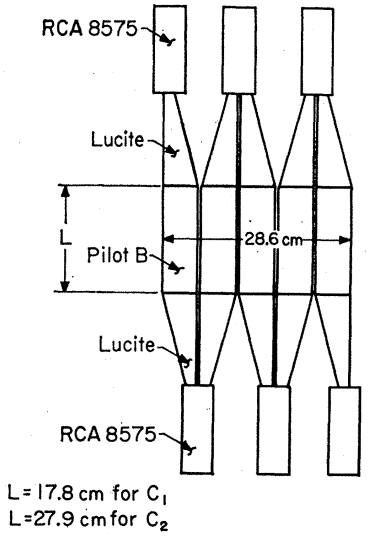

FIG. 5. Scintillator and photomultiplier tube arrangement for time-of-flight counters C_1 and C_2. The scintillator was viewed at opposite ends for improved time resolution.

(TAC), discussed later. The 3-of-6 veto, shown in Fig. 6, canceled any event where two particles passed through two different scintillators of the same counter within about 20 nsec of each other. This helped to reduce accidental coincidences where an initial particle could trigger only C_1 and a later particle, less massive than the deuteron, could traverse the complete TOF telescope and fake a deuteron. The local logics for C_3 consisted of merely gating the upper tube and the lower tube, separately, by the same upper-lower coincidence before transmitting them to the main logics.

Figure 7 is a block diagram of the main logics. The TOF was measured twice, over the complete flight path of 17.7 m by a C_1C_3 coincidence and over the last 8.84 m of the flight path by a C_2C_3 coincidence. An event required a coincidence between the two TOF measurements. Therefore, counters C_1 and C_3 and counters C_2 and C_3 were combined in parallel circuits in both the slow section, using conventional coincidence techniques, and the fast section, using TAC's. In the slow section, raw $C_1C_2C_3$ coincidences were scaled down by powers of 10 (usually 1000) and brought back into coincidence with both a C_1C_3 and a C_2C_3 coincidence, which were set to accept everything: pions, kaons, protons, and deuterons. Eventually, there was formed an unscaled slow threefold coincidence timed for deuterons only (S123D) and a scaled slow threefold coincidence which included everything except deuterons (S123P). The slow section required only the upper tubes of the TOF counters.

The fast electronic circuitry was designed to minimize the effects of the vertical-position spread in the counters in the manner suggested, that is, measuring the TOF between the same pairs of counters twice and adding

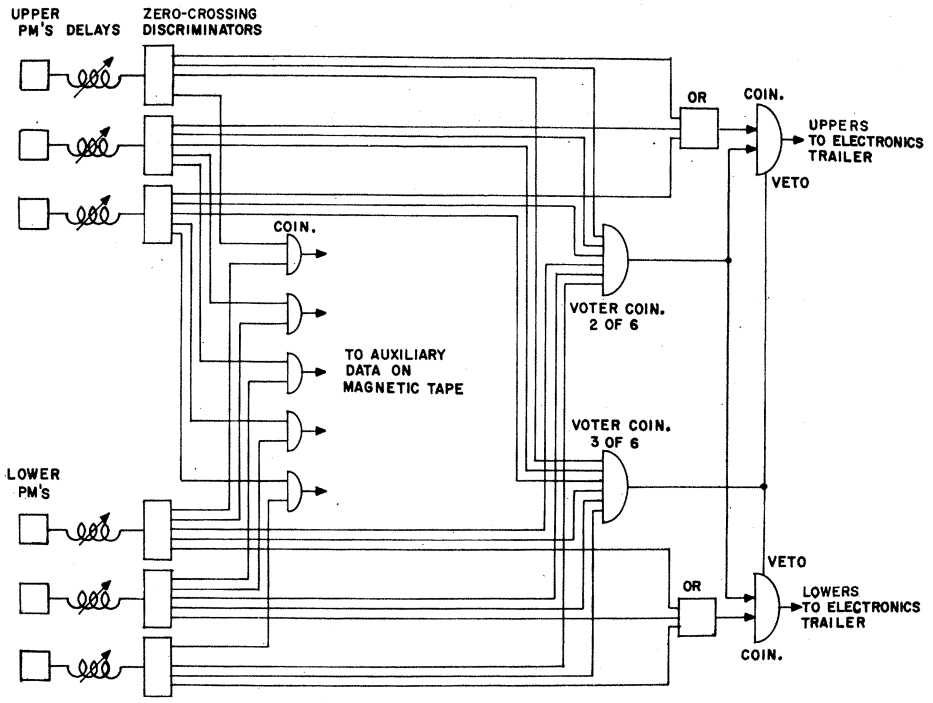

FIG. 6. Block diagram of the electronic circuitry for either time-of-flight counter C_1 or C_2. This system of local logics was placed in close proximity (1.5–3 m) to each counter.

the resulting measurements. Accordingly, the upper tubes were used to trigger one coincidence circuit (overlap mixer) and its accompanying TAC, while the lower triggered a parallel circuit. The outputs of the upper and lower TAC's were added in a linear mixer. The output of the linear mixer, after amplification, was sent to an analog-to-digital converter which was triggered by the event. The TOF for each event was subsequently recorded on magnetic tape. This procedure was followed for both the C_1C_3 and the

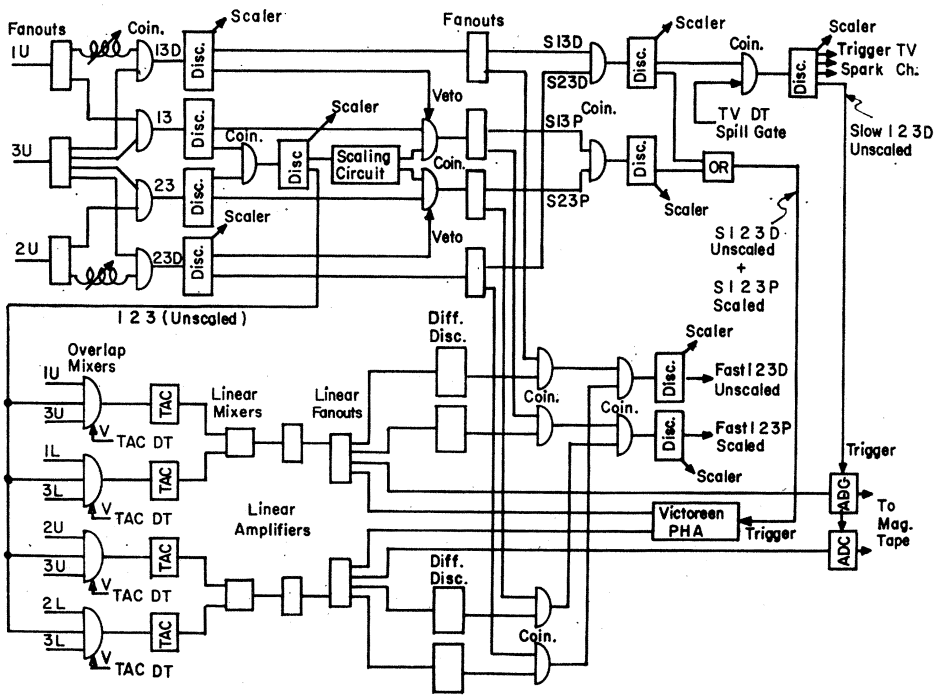

FIG. 7. Block diagram of the main logics located in the electronics trailer.

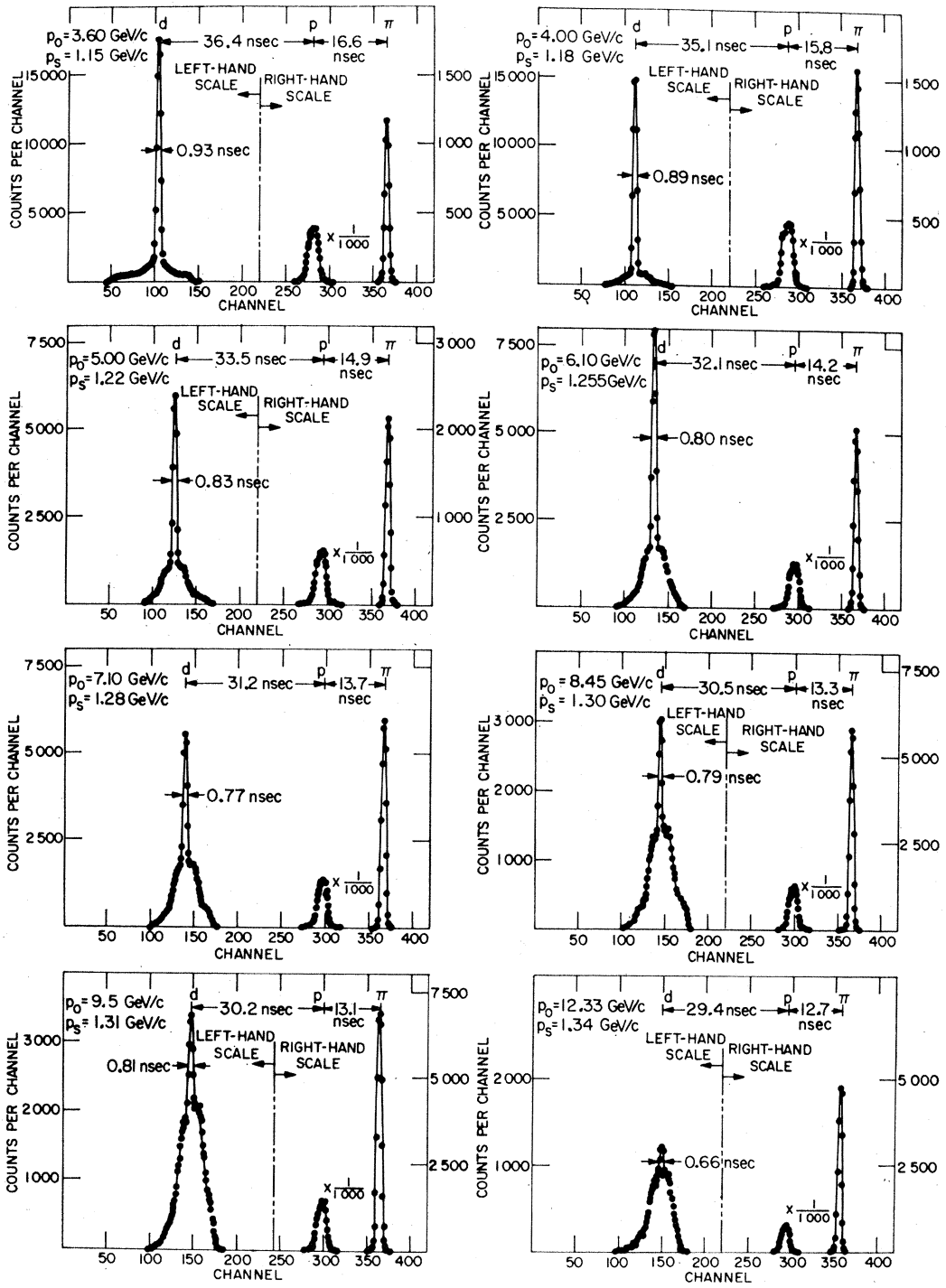

FIG. 8. Sample time-of-flight spectra showing the deuteron, proton, and pion peaks, the latter two scaled by a factor of 1000. The time separation between the peaks corresponds to a flight path of 17.7 m. Five channels correspond to 1 nsec.

C_2C_3 TOF measurements. The output of the linear mixer for the C_1C_3 TOF measurement was also recorded in a pulse-height analyzer (PHA) which was gated by an S123D unscaled and an S123P scaled. As expected, this "balanced TAC" technique proved superior to simply ORing the upper and the lower tubes together before sending them to the overlap mixer, a possibility explored during the experiment.

Figure 8 shows sample TOF spectra as recorded in the PHA for incident proton momentum $p_0=3.6$–12.3 GeV/c. These spectra are for the total flight path of 17.7 m. The proton and pion peaks, scaled by a factor of

1000, appear on the right and the deuterons on the left. The sharp peak, corresponding to the deuterons from reaction (1), has an average full width at half-maximum (FWHM) over many runs of 0.8 ± 0.1 nsec. It is superimposed on a broad distribution due to non-hydrogen background. The sharpness of the peak is due to the fact that the experiment was performed in the flat region of the p_d–θ_d diagram of reaction (1) where p_d is almost constant (see Fig. 1).

The TV and spark chambers were triggered by an S123D. For the range of spectrometer momenta covered in this experiment, the deuteron-proton TOF difference varied from 14.7 to 18.4 nsec for the 8.84-m flight path, and the S123D was more than adequate to separate out the deuterons. The total delay from the passage of a particle through C_3 until an S123D signal was available in the electronics trailer was about 300 nsec.

A glycerol threshold Čerenkov counter, whose dimensions were 30.5 cm×30.5 cm×5.7 cm, was placed at the end of the spectrometer after C_3. With a refractive index of 1.473, the minimum momentum for the production of Čerenkov radiation in glycerol is 0.13, 0.87, and 1.73 GeV/c for pions, protons, and deuterons, respectively. In the momentum range 1.14–1.34 GeV/c, the rejection efficiency of the Čerenkov counter was measured and found to be 97, 70, and 8% for pions, protons, and deuterons, respectively. The Čerenkov counter was gated by C_3 at the local logics, eventually strobed by a deuteron event, and placed on magnetic tape for future cross checking of the identification of deuterons by TOF. The Čerenkov counter was not used in the selection of events.

E. Gating and Dead Time

The logics were gated to count only during the flat portion of the ZGS "front porch." This was accomplished in part using signals made available to the experimenter from the ZGS control room.

In order to reduce multiple tracks in the chambers, a pileup gate requirement was placed on the events. The "singles" counts from counter C_1 were fed to the input of a pileup gate which generated a continuously updated gating level until 1 μsec had elapsed between particles in C_1. This gating level blocked the events which could give multiple tracks. The number of these varied from a few percent to as much as 40% of the events.

The television system, the spark chambers, and the electronic circuitry were all subject to an insensitive period or dead time, following activation, during which they could not accept further tasks. The actual TV dead time was 8 msec and will be discussed in Sec. II F. However, because of spark-chamber deterioration, it was found best not to run the spark chambers much faster than 60 triggers per second. Therefore, the TV spark-chamber dead time was set at 15 msec per event by a gate generator.

The dominant sources of dead time in the electronic circuitry were the TAC's and the "singles" counts in the TOF counters. The TAC's had a dead time of 10 μsec which was fixed by a gate generator. The output of this gate generator and the pulses from C_1, C_2, and C_3 were combined to form an electronic dead-time veto signal.

All gating and dead-time losses were monitored and recorded throughout the experiment. The TV spark-chamber dead-time losses were accounted for by counting monitor M_1 before and after application of the TV spark-chamber dead-time gate. The pileup gate losses were accounted for by counting the number of events (S123D) before and after application of the pileup gate. Finally, the electronic dead time was accounted for by counting M_1 before and after application of the electronic dead-time veto signal. The quantities discussed above, plus many others required for data reduction or control of the experiment, were displayed on 100-MHz scalers and recorded by taking photographs of them at the end of each run, in addition to being continuously recorded on magnetic tape.

F. Spark Chambers and Vidicon Readout

The spark chambers with automatic vidicon readout were essentially the same as those used in an earlier experiment at the ZGS[15] and described elsewhere.[16] However, several changes were made to the system in order to handle the higher event rate. The most significant of these changes included the reduction of the number of scanning lines per view from 30 to 8, the reading of the chambers in parallel rather than in serial, and the inclusion of a buffer memory between the digitizer and the magnetic tape unit. The buffer memory was required so that the magnetic tape unit, with its relatively slow mechanical drive, would not limit the number of events recorded per ZGS pulse. In the new arrangement the magnetic tape unit was activated only between ZGS pulses and then received the events stored in the buffer memory.

The 25.4-cm×25.4-cm spark chambers had six 7.6-mm gaps consisting of seven planes of 13-μ aluminum foil. The chambers were operated at about 10 kV. The gas mixture (90% neon, 10% helium) flowed continuously through the chambers at about 5 cm^3/sec and exhausted to the atmosphere after passing through an oxygen analyzer. The chambers were pulsed using EGG high-voltage pulsers (HV100) and hydrogen thyratrons (HY10). The total delay from the time a

[15] H. L. Anderson, S. Fukui, D. Kessler, K. A. Klare, M. V. Sherbrook, H. J. Evans, R. L. Martin, E. P. Hincks, N. K. Sherman, and P. I. P. Kalmus, Phys. Rev. Letters **18**, 89 (1967).

[16] H. L. Anderson and A. Barna, Rev. Sci. Instr. **35**, 492 (1964); E. P. Hincks, H. L. Anderson, H. J. Evans, S. Fukui, D. Kessler, K. A. Klare, J. W. Lillberg, M. V. Sherbrook, R. L. Martin, and P. I. P. Kalmus, in *Proceedings of the 1966 International Conference on Instrumentation for High Energy Physics, Stanford* (International Union of Pure and Applied Physics and U. S. Atomic Energy Commission, Washington, D. C., 1966), p. 63.

particle passed through C_3 until the chambers were pulsed was about 570 nsec. This included the 300-nsec delay in forming the triggering pulse (S123D) mentioned earlier, 50-nsec cable delay from the electronics trailer to the HV100 at the local logics, 50-nsec delay through the HV100, 20-nsec cable delay from the local logics to the spark chambers, and about 150-nsec delay in the hydrogen thyratron at the spark chambers. A constant 15-V clearing field was maintained on the chambers to sweep away residual electrons. In order to increase the spark-chamber memory time for good events, a coincidence between C_1 and C_2, timed for deuterons only, was formed at the local logics to turn off the clearing field on all chambers in about 50 nsec from the time a deuteron passed through C_2.

Figure 9 shows a spark chamber with its optical system for imaging both orthogonal views on one vidicon. The system utilized a series of first-surface mirrors and 90° bends to direct both spark-chamber views to the camera lens, one above the other. In addition, there was a field lens, beam splitter, and fiducial pattern associated with each view. The fiducial pattern consisted of a mask with a series of parallel slits illuminated with light from incandescent lamps, which could be switched on when needed. The beam splitters were partially aluminized 6.4-mm glass plates, set at 45° to both the spark chamber and the fiducial pattern. The beam splitters served to reflect some of the light from the fiducial marks (about 40% from the first surface) into the optical system. They also wasted about half the light from the sparks, but this was acceptable. The fiducial patterns were accurately located with respect to the housing which contained the spark chamber and optical system. Data taking was interrupted about every $\frac{1}{2}$ h or 5000 events and the fiducial marks recorded on the magnetic tape in the same manner as the particle tracks.

The spark-chamber readout system could handle up to eight television cameras and consisted of a TV monitor, a digitizer, a magnetic core storage buffer, a magnetic tape unit, and a storage display tube readout. The system had a capacity of four sparks per chamber with an indication of overflow if more than four sparks occurred. Each view was digitized eight times and with two views per camera and up to eight cameras a total of 128 words of memory per event was required. The buffer storage unit was a Nanomemory 900 with a capacity of 8192 65-bit words. Therefore, the memory had a potential capacity of 64 events per ZGS beam spill. The television system was a modified closed circuit system utilizing a 21-line noninterlaced frame. The horizontal sweep was 62.5 μsec per line. The vertical period was 1.31 msec and the aspect ratio was approximately 2 to 5. Five lines were used for vertical retrace and 16 lines for digitization of the spark images. All eight cameras were driven in parallel by the digitizer using signals derived from the countdown circuitry

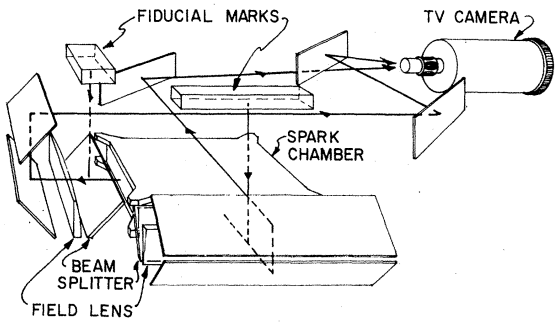

FIG. 9. Spark chamber and optical system for imaging both orthogonal views on one vidicon.

of a 20-MHz clock. After the vidicon signal passed through a zero-crossing circuit, the spark image was digitized by stopping the first of four scalers which had started counting pulses from the 20-MHz clock at the beginning of the scan line. There were about 1000 addresses per line so that each address corresponded to about $\frac{1}{4}$ mm in real space for 25.4-cm spark chambers. Additional sparks would stop the second, third, and fourth scalers.

During horizontal flyback, eight words were serially read into the buffer memory. Each word consisted of 44 bits from the four digitizing scalers, eight bits of auxiliary data, and seven flag bits. With 128 words per event the system could handle 36 seven-decade BCD auxiliary data devices. Auxiliary data included clock time, run number, event number, hodoscope information, Čerenkov-counter identification, TOF, digital voltmeter (DVM) readings of magnet currents, and all scaler quantities necessary for the proper normalization of the data. At the end of a beam spill, the accumulated data was read from the memory and written on magnetic tape using IBM compatible format at a density of 556 bits per in. at a rate of 62 500 characters per sec. The read head of the tape unit was coupled to a reconstructor which could display one event at a time on a storage display tube. This device served as an over-all system monitor. The TV dead time, including four frames for erasing the vidicons, was about 8 msec. However, as noted earlier, the dead time was set at 15 msec, thus limiting the system to a maximum of 33 events in a 500-msec beam spill. Typically, with 10^{11} protons/pulse about 15 to 25 events were recorded in a 500-msec spill. It took about 2 to 3 h to fill a magnetic tape with 30 000 events. This included time for writing fiducial marks on the magnetic tape, recording data, changing tapes, and filling or emptying the hydrogen target.

III. ANALYSIS

A. Processing of Magnetic Tapes

The magnetic tapes were processed on the University of Chicago IBM-7094/7040 and the Los Alamos Scientific Laboratory CDC-6600 computers. The

fiducial marks and spark-chamber tracks were reconstructed by a pattern-recognition program from the digitized coordinates on magnetic tape. The fiducial pattern was used to establish a third-order relation between the digitized vidicon output and coordinates in real space. The quadratic term in this expression was found to be small and due to nonlinearities in the spark-chamber optics and TV horizontal sweep. The calibration was updated about every 5000 events, a procedure which was found by experience more than adequate to compensate for small long-term drifts in the vidicon system.

The program required at least one track in three or more of the five spark chambers, one of which had to be SC_1 or SC_2. The combination SC_2, SC_4, SC_5 in the horizontal plane (X), having a poor momentum determination, was also rejected and counted with the category of "three or more chambers missing." These events comprise a spark-chamber or vidicon inefficiency.

Where allowed, the event was successively tried with five, four, and three chamber combinations. The goodness-of-fit (χ^2) calculation and retrace to the target were performed for each combination. For three chambers in X, there is no χ^2. To determine the χ^2 an error matrix was calculated. To a ± 0.35-mm uncertainty in spark position (including such factors as digitization resolution, vidicon drift, spark drift, and alignment uncertainty) were added the correlated errors (calculated at the central momentum) due to multiple scattering in the foils, gases, and counter C_2. The transport equations were inverted in a minimum-χ^2 sense using this error matrix for weighting. A matrix for calculating χ^2 and one for the position, angle, and momentum values were determined for use with each combination of spark chambers. The order in trying the combinations was determined by errors expected in momentum and retrace, the best being taken first. The size of the errors was confirmed by the χ^2 distributions found.

A combination was considered as having no retrace if its calculated target position had a probability less than 0.1% (0.5% for three chambers in X). Trajectories with no retrace were classified as nonhydrogen events and rejected. An event was declared to have multiple solutions in X if for the same number of chambers the second best combination of chambers or tracks also had a probability greater than 0.1%. Events with multiple solutions were classified as ambiguous and considered a spectrometer analysis inefficiency. An event had no solution if no combination had a χ^2 probability greater than 0.1% (0.5% for three chambers). Events with no solution were classified as accidental coincidences and rejected. A four- or five-chamber event for which there was no retrace but that had a χ^2 probability greater than 0.1% was declared no retrace. A four- or five-chamber event which had a χ^2 probability greater than 0.5% was accepted without testing the other combinations.

Subsequently, an event would be rejected as bad if the measured and calculated TOF of either the C_1C_3 or C_2C_3 combination differed by more than 3 nsec, the position at C_3 was more than 16 cm from the center, the position at the collimator was horizontally (vertically) more than 8 (12) cm from the center, or the measured or calculated positions at the spark chambers was more than 12.7 cm from the center.

Having passed all selection criteria, an event was classified as good and the momentum and angle of emission of the deuteron calculated. After correcting for the energy loss of the deuteron in the spectrometer, the program computed the missing mass squared (MM^2). Since the position of the vertex in the target is indeterminate, the program could not correct for the energy loss of the deuteron in the target.

While providing the important MM^2 distribution, the program provided considerable additional information necessary for the proper control of the experiment, maintence of equipment, and analysis of the results. Although not used, the program was capable of placing additional selection criteria on the events, such as hodoscope or Čerenkov requirements.

Figure 10 presents sample MM^2 spectra in the pion region for incident proton momentum in the range $p_0 = 3.6$–12.3 GeV/c. As indicated in Fig. 10, the experimentally measured spectrometer resolution (FWHM) in missing-mass squared, $\delta(MM^2)$, increases from 0.028 GeV^2 at 3.6 GeV/c to 0.096 GeV^2 at 12.3 GeV/c. A calculation of $\delta(MM^2)$, including the uncertainties from the incident proton momentum and angle, the uncertainty due to the energy loss of the deuteron in the target, and the deuteron momentum and angle measurement errors, yields a FWHM of 0.030 GeV^2 at 3.6 GeV/c and 0.102 GeV^2 at 12.3 GeV/c, in good agreement with the experimentally observed values. The momentum measuring error (about $\pm\frac{1}{3}$%) was the single largest contributor to the uncertainty in the MM^2 and was usually about twice the contribution from the energy loss of the deuterons in the target.

The peak in the MM^2 spectra centered at 0.02 GeV^2 is clearly due to deuterons from reaction (1). The background, indicated by the target-empty points, comes from the target walls and the radiation shield. An additional background effect, which is evident above and below the $d\pi^+$ peak, comes from deuterons produced in the walls of the vacuum pipe by secondary particles from the hydrogen in the target. Accidental coincidences simulating deuterons do not appear to contribute to the spectra. Accidental coincidences between the C_1C_3 and C_2C_3 TOF measurements were counted during the experiment and found to be negligible.

B. Normalization and Summation of Spectra

To obtain the differential cross section for reaction (1) from the MM^2 spectra, it was necessary to normalize each run to the M_1 monitor, make the corrections for

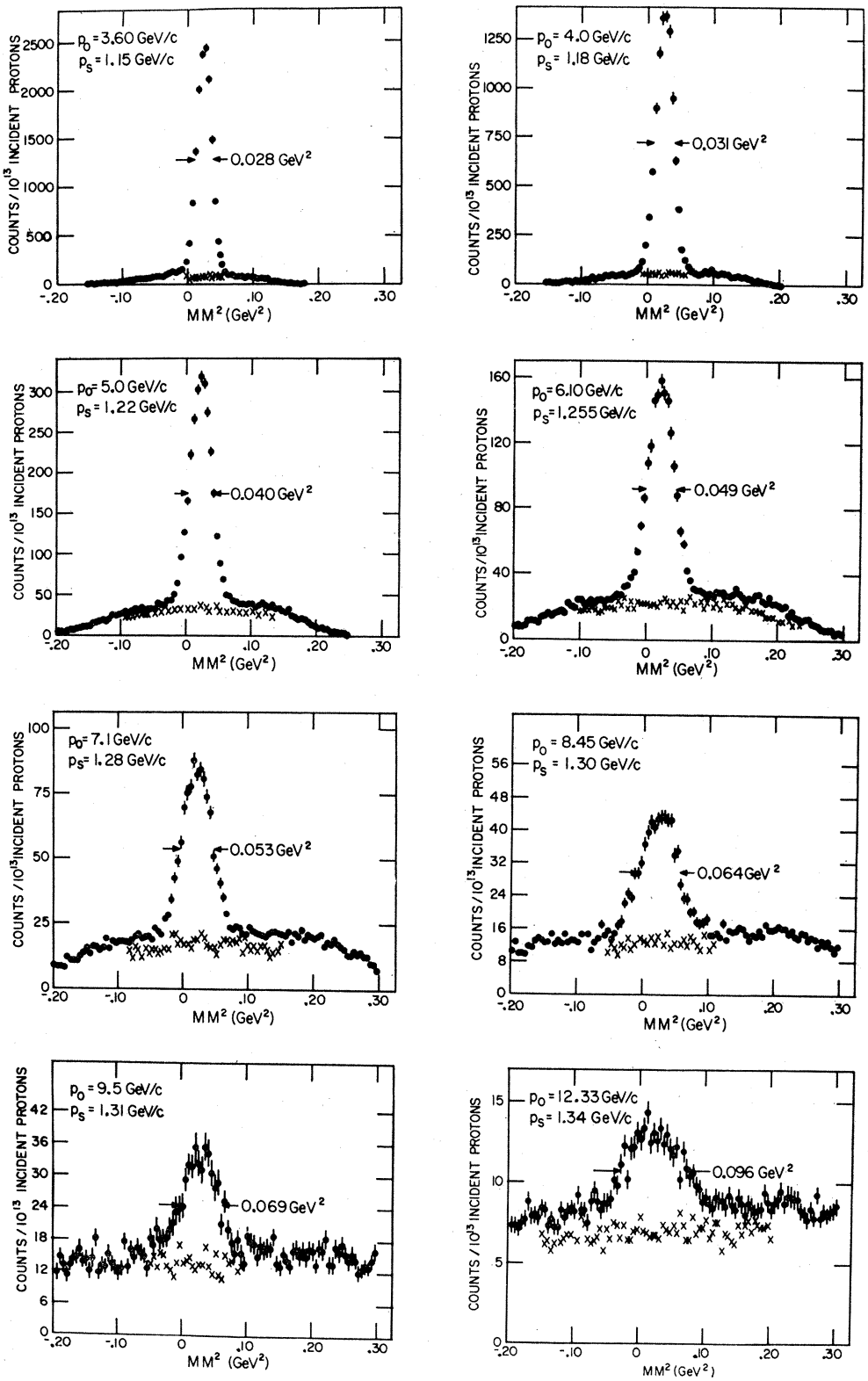

FIG. 10. Sample missing-mass squared spectra in the pion region. The upper (circles) and lower (crosses) spectra show the target-full and target-empty data, respectively, normalized to the same number of incident protons.

spectrometer inefficiencies and logic dead time, and correct the spectra for the spectrometer momentum acceptance as calculated by the Monte Carlo program and shown in Fig. 4. This made it possible to add spectra taken at the same incident momentum p_0 but different settings of the spectrometer. The number of corrected events $\Delta\nu_f$ ($\Delta\nu_e$) for the target full (empty) within a given bin of the MM^2 histogram was calculated from the formula

$$\Delta\nu_f\,(\Delta\nu_e)=\frac{G_f\,(G_e)}{\epsilon_\alpha\epsilon_\beta\epsilon_\gamma\epsilon_\delta\epsilon_\epsilon \mathrm{M}_1}, \tag{2}$$

where G_f (G_ϵ) is the number of events in a given bin of the MM^2 histogram for the target full (empty) and passing all criteria of the event-analysis program, ϵ_α is the combined efficiency of the spark chambers and vidicon cameras using chamber redundancy, ϵ_β is the spectrometer analysis efficiency due to the ambiguity of events with too many good solutions in the horizontal plane, ϵ_γ is the correction for the pileup gate losses, ϵ_δ is the correction for the electronic dead-time losses, ϵ_ϵ is the spectrometer efficiency over the accepted momentum interval as calculated by the Monte Carlo program (including the estimated loss of deuterons due to multiple scattering), and M_1 is the total number of monitor M_1 counts recorded after application of the TV spark-chamber dead-time gate. The spectrometer efficiencies ϵ_α and ϵ_β were computed for each run from the event rejection categories and were typically 0.995 and 0.98, respectively. The pileup gate efficiency ϵ_γ, the electronic dead-time correction ϵ_δ, and the M_1 counts were computed from the appropriate auxiliary data for each run. Both ϵ_γ and ϵ_δ were strongly rate dependent and varied greatly from run to run depending upon the EPB intensity and whether the target was full or empty. Consequently, ϵ_γ ranged from 0.60 to 0.95 and ϵ_δ from 0.90 to 0.99. Finally, the usable portion of the spectra was restricted to the interval differing by $+4.5\%$ to -3.9% from the central momentum. This gives a spectrometer efficiency of at least 30% (see Fig. 4).

Because of the slightly larger nonhydrogen background present during the target-full runs, the target-empty runs were normalized to the target-full runs in the nonphysical region (negative MM^2) and then subtracted. What remained was a prominent peak due to single-pion production superimposed on a contribution due to multipion production, slowly rising with energy. In our preliminary analysis[1] of the data we simply drew the background by eye as a straight-line fit to the data above and below the peak, and ascribed to single-pion production the sum total of events in the peak above the straight line. Subsequently, we analyzed the data above the pion peak in much more detail. For several values of our incident momentum we took a continuous MM spectrum to $MM^2 \geqslant 1.6$ GeV^2. This enabled us to make a more detailed evaluation of the multipion contribution. The data above the pion peak were dominated by a broad maximum due to ρ production on a smoothly rising background, which we took to be the contribution according to phase space of 2π, 3π, and $\pi\rho$ production. The analysis of this part of the data will be described in a subsequent publication. We mention it here because we used it to make a more accurate subtraction of the multiparticle background under the pion peak. After this subtraction, we obtained good fits of the pion peak with a Gaussian distribution, the integral of which gave the event rate ν.

The refined analysis had an inappreciable effect on the cross sections for low values of p_0 where the background was quite small in any case. The new background subtraction gave cross sections which were generally higher but by less than 5%, except for the values at $p_0=6.20$, 6.85, 7.90, 8.45, 9.00, 11.00, and 12.33 GeV/c, where the increases were by 6.4, 6.5, 22.8, 7.4, 6.6, 6.3, and 23.7%, respectively.

C. Calibration of Monitor M_1

It was noted earlier that the M_1 monitor counts were related to the number of incident protons by gold-foil activation. A calibration run consisted of exposing a 15.2-cm×15.2-cm×13-μ foil at the SEM_2 stand for about 4 h while the experiment was in progress. During the bombardment, the total number of M_1 counts, the time of exposure, and any changes in relative intensity of the EPB were recorded. A radioautograph of the foil was taken after exposure to determine the beam size at the SEM_2 stand and the proper cutting pattern of the foil. About 4 h after the end of the foil exposure, the α particles were counted in calibrated windowless flow-type proportional counters. The number of protons Q incident upon the foil was calculated from this measurement and the known cross section for the production of the α branch of Tb^{149} from Au. Figure 11 shows this cross section as a function of proton kinetic energy T_0. The curve shown is a least-squares fit to the data of Franz and Friedlander[17] for the range of proton energies of interest in this experiment and to the one point of Steinberg *et al.*[14] at 11.5 GeV. There is a $\pm 5\%$ normalization uncertainty in these data which is not included in the errors of our differential cross sections for reaction (1).

At least one gold foil was exposed at most of the EPB momenta studied in this experiment and 13 calibrations were made at 12.3 GeV/c, providing a good check on the internal consistency of the measurements. The reproducibility of the calibrations depended to a great extent upon the foils receiving scrupulous attention and handling from initial bombardment to final counting of the α particles. This required keeping an accurate log of the exposure time and any relative changes in the EPB intensity. Since for counting purposes the foils were not to exceed about 6.5 cm^2, the large beam size at the SEM_2 stand (up to 10 cm in

[17] E. M. Franz and G. Friedlander, Nucl. Phys. **76**, 123 (1966).

diam) required a rather complex cutting pattern of the exposed foil. This in turn generated a great number of foil sections which had to be carefully cut, mounted, and electrically grounded to metal disks. Deviations from the standard procedure resulted in very unreliable measurements. Also, the large beam size at SEM_2 made it difficult to collect all the protons in the EPB. Figure 12 shows the ratio M_1/Q versus p_0 for all calibrations taken during the experiment; also shown is the least-squares fit that was made to these data. From the internal consistency of the 12.3-GeV/c points, we determined the calibration error to be $\pm 3.4\%$, and folded this in to the other errors of the measurement.

IV. CORRECTIONS TO DATA

Target-full and target-empty runs were taken at each measurement of the differential cross section and the background removed by subtraction. A correction was applied for the residual H_2 gas in the empty target. A definite warming effect of the target was noted during target-empty runs, usually 1 h long, from the decrease of the M_2 rate with time. This decrease, about 2–4% of the target-empty effect, was due to the decrease of the H_2 gas density with rising temperature. The target-empty temperature was assumed to be $(35\pm 15)°K$, giving a net H_2-gas effect of $(1.1\pm 0.5)\%$ of the liquid-H_2 effect.

Since the H_2 target was a vertical cylinder, most of the proton beam did not traverse the full diameter. The reduction in length was by a factor of 0.980 ± 0.008, obtained by averaging over a horizontal beam width of 2.5 ± 0.5 cm.

There was a slight attenuation of the proton beam in traversing the hydrogen target. Since the EPB intensity was measured downstream of the hydrogen target, the above considerations resulted in a correction increasing the beam intensity by a factor of 1.007.

Deuterons were lost by multiple Coulomb scattering and nuclear interactions. As mentioned earlier, the Monte Carlo program was used to estimate the amount

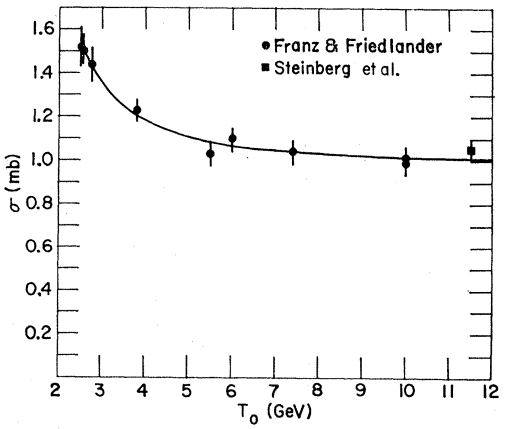

FIG. 11. Cross section σ for production of the α branch of Tb^{149} from Au by proton bombardment as a function of incident proton kinetic energy T_0. The curve represents a least-squares fit to the data of Ref. 14 (square) and Ref. 17 (circles).

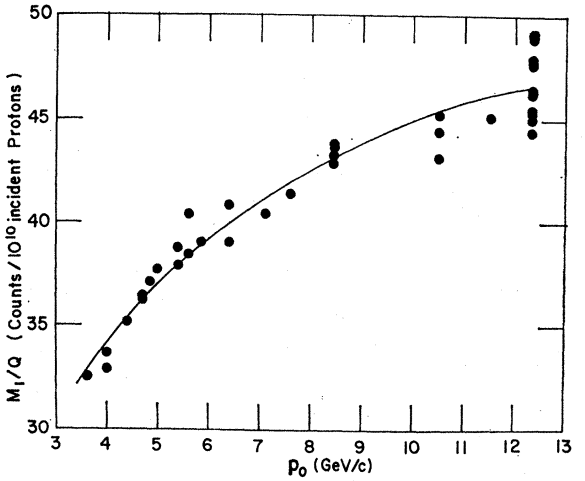

FIG. 12. Ratio of monitor M_1 counts to the number of incident protons Q as a function of incident proton momentum p_0. The protons were counted using the gold-foil technique (see Ref. 14). The curve is a least-squares fit to all calibration measurements taken during the experiment.

of multiple scattering within the spectrometer. It was found that the correction to be applied ranged from 0.953 ± 0.005 at the lowest spectrometer momentum to 0.987 ± 0.005 at the highest. An estimate of the deuteron loss due to nuclear interactions can be made from a knowledge of the amount and type of material in the deuteron path (hydrogen target, helium, air, Mylar windows, counters, and spark chambers) and from the deuteron-nucleon cross section σ_{dN}. The cross section for the various absorbers was approximated by $\sigma_{dA}=\sigma_{dN}A^{2/3}$, where σ_{dN} ranges from 74 mb at the lowest deuteron momentum of interest to 62 mb at the highest.[18] This resulted in a transmission probability which ranged from 0.953 to 0.959 ± 0.010.

The over-all counting efficiency ϵ_e was defined to include the detection efficiency of the TOF counters, the dead time of the zero-crossing discriminators at the local logics, and the 3-of-6 veto rate at the local logics. The detection efficiency of the counters was measured using protons and pions in the spectrometer beam. Two trigger counters (6.5 cm^2) were placed on opposite sides of the TOF counter to be studied and the efficiency determined as a function of position. An estimate of the dead time in counter C_1 was made by assuming an average of 10^5 particles/pulse in C_1 and an average beam spill of 500 msec. During the experiment, the 3-of-6 veto rate in C_1 was continuously recorded and 2.9% found to be a good average value. The dead time and 3-of-6 rate in C_2 were estimated from a knowledge of the relative counting rates in C_1 and C_2. The dead time in C_3 was negligible and C_3 had no 3-of-6 veto. The over-all counting efficiency was found to be $\epsilon_e=0.96\pm 0.02$. The relatively large uncertainty is due primarily to the dependence of the dead time and 3-of-6 veto effect upon the EPB rate.

[18] F. F. Chen, C. P. Leavitt, and A. M. Shapiro, Phys. Rev. 103, 211 (1956).

V. RESULTS

The differential cross section for reaction (1) in the c.m. system was calculated from the formula

$$\left(\frac{d\sigma}{d\omega}\right)_{\text{c.m.}} = \frac{\nu}{(Q/M_1)\rho d(d\omega/d\Omega)\Delta\Omega\epsilon_a\epsilon_b\epsilon_c\epsilon_d\epsilon_e}, \quad (3)$$

where ν is the number of events in the pion peak as obtained from the analysis program Q/M_1 is the number of protons traversing the target normalized to monitor M_1, ρ is the density of liquid hydrogen (4.23×10^{22} protons/cm^3), d is the diameter of the target (7.43 ± 0.08 cm), $d\omega/d\Omega$ is the solid-angle transformation from the laboratory to the c.m. system, $\Delta\Omega$ is the laboratory solid angle of the spectrometer (2.08×10^{-4} sr), ϵ_a is the correction for the residual hydrogen gas in the target (0.989 ± 0.005), ϵ_b is the correction to the target diameter (0.980 ± 0.008), ϵ_c is the correction for the attenuation of the proton beam in the target, (1.007), ϵ_d is the transmission probability of deuterons due to nuclear interactions (0.953 to 0.959 ± 0.010 depending on momentum), and ϵ_e is the counting efficiency (0.96 ± 0.02). With the exception of the counting efficiency ϵ_e which is rate dependent, the uncertainties in the corrections listed above introduce systematic errors in the differential cross sections. When combined quadratically with the $\pm5\%$ uncertainty in the cross section for the production of Tb^{149} α particles in gold, they yield a $\pm5.3\%$ normalization error in our differential cross sections. The nonstatistical error in the relative differential cross sections arises from a $\pm0.8\%$ error in the laboratory to c.m. transformation due to the uncertainty in the beam energy, the $\pm2\%$ uncertainty in the counting efficiency ϵ_e, and the $\pm3.4\%$ uncertainty in the gold-foil calibration. These errors, when combined quadratically, contribute $\pm4.1\%$ to the error in the differential cross sections for reaction (1). These differential cross sections in the c.m. system, obtained from the MM spectra, are presented in Table I. The uncertainties shown are compounded from the $\pm4.1\%$ error and the statistical error, but they do not include the $\pm5.3\%$ normalization error.

TABLE I. Measured c.m. differential cross section for the reaction $p+p\rightarrow d+\pi^+$.

p_0 [a] (GeV/c)	p_d [b] (GeV/c)	$\cos\theta_{\text{c.m.}}$	s [c] (GeV^2)	$(d\sigma/d\omega)_{\text{c.m.}}$ [d] (μb/sr)	$(d\sigma/d\omega)_0$ [e] (μb/sr)
3.40	1.140	0.9928	8.38	14.96 ±0.67	...
3.60	1.154	0.9934	8.74	13.57 ±0.58	19.98 ±0.85
3.85	1.169	0.9940	9.20	11.72 ±0.48	17.38 ±0 71
4.00	1.177	0.9943	9.47	10.44 ±0.48	15.55 ±0.71
4.40	1.197	0.9950	10.20	6.68 ±0.29	10.05 ±0.44
4.70	1.210	0.9954	10.75	4.74 ±0.22	7.19 ±0.33
4.85	1.216	0.9956	11.03	3.87 ±0.17	5.88 ±0.26
5.00	1.221	0.9957	11.31	3.47 ±0.15	5.30 ±0.23
5.15	1.226	0.9959	11.58	3.05 ±0.14	4.70 ±0.22
5.35	1.233	0.9961	11.96	2.76 ±0.13	4.24 ±0.20
5.60	1.241	0.9963	12.42	2.65 ±0.13	4.09 ±0.20
5.85	1.248	0.9965	12.88	2.50 ±0.12	3.89 ±0.19
6.00	1.252	0.9966	13.16	2.63 ±0.16	4.10 ±0.25
6.10	1.254	0.9967	13.34	2.51 ±0.12	3.91 ±0 19
6.20	1.257	0.9967	13.53	2.48 ±0.16	3.88 ±0.25
6.30	1.259	0.9968	13.72	2.51 ±0.16	3.93 ±0.19
6.40	1.261	0.9969	13.90	2.40 ±0.13	3.76 ±0.20
6.85	1.271	0.9971	14.73	2.12 ±0.22	3.35 ±0.35
7.10	1.276	0.9972	15.20	1.62 ±0.09	2.57 ±0.14
7.35	1.280	0.9973	15.66	1.50 ±0.18	2.38 ±0.29
7.60	1.285	0.9974	16.13	1.47 ±0.08	2.35 ±0.13
7.90	1.290	0.9976	16.69	1.40 ±0.21	2.25 ±0.34
8.45	1.297	0.9977	17.71	1.15 ±0.06	1.86 ±0.10
9.00	1.305	0.9979	18.74	0.922±0.066	1.50 ±0.11
9.50	1.310	0.9980	19.67	0.864±0.078	1.42 ±0.13
10.50	1.320	0.9982	21.54	0.664±0.063	1.11 ±0.11
11.00	1.324	0.9983	22.48	0.558±0.062	0.934±0.104
11.50	1.328	0.9984	23.41	0.491±0.058	0.827±0.098
12.33	1.335	0.9985	24.96	0.438±0.047	0.744±0.080

[a] Laboratory momentum of the incident proton.
[b] Laboratory momentum of the deuteron.
[c] Square of the total c.m. energy.
[d] Differential cross section at $\theta_{\text{lab}}=5°$. A normalization error of $\pm5.3\%$ has not been incorporated in these results.
[e] Differential cross section extrapolated to exactly 0° as discussed in the text.

Table I. The values listed here differ only in minor ways from those used for the plot given in our original publication.[1] Here we give the incident proton laboratory momentum p_0, the laboratory momentum of the observed deuteron (central value) p_d, the cosine of the c.m. production angle corresponding to the fixed 5° (central value) laboratory angle at which the deuteron was observed, and the square of the total c.m. energy. Next we give the differential cross sections as calculated from the MM spectra and, finally, the differential cross sections extrapolated to exactly 0° in the manner discussed below.

As was noted earlier, the differential cross sections could also be extracted from the TOF data, corresponding to a pure counter experiment. This was possible for reaction (1) because of the very favorable signal-to-background ratio, which is evident in the typical TOF spectra shown in Fig. 8. The differential cross sections were computed from the TOF data using only the target-full runs. The only deuterons present in the TOF spectra originating from the liquid hydrogen were those of reaction (1). Therefore, the background was subtracted from the TOF spectra by fitting a quadratic relation to the nonhydrogen deuterons in a selected region above and below the sharp peak corresponding to deuterons from reaction (1). This was found to be more reliable than either a linear fit or a subtraction of target-empty runs. The over-all agreement between the TOF and MM cross sections was very good, with most measurements agreeing within a few percent. A few of the high-momentum points showed individual deviations as high as 19%; however, in this region the TOF signal-to-background ratio is far less favorable and those large deviations are probably due to the uncertainties in the TOF background subtraction.

VI. DISCUSSION

The differential cross sections for the process $p+p\rightarrow d+\pi^+$ obtained in this experiment are given in tabular form in Table I. The values listed here differ only in minor ways from those used for the plot given in our original publication.[1] Here we give the incident proton laboratory momentum p_0, the laboratory momentum of the observed deuteron (central value) p_d, the cosine of the c.m. production angle corresponding to the fixed 5° (central value) laboratory angle at which the deuteron was observed, and the square of the total c.m. energy. Next we give the differential cross sections as calculated from the MM spectra and, finally, the differential cross sections extrapolated to exactly 0° in the manner discussed below.

As a function of incident momentum, our cross sections decrease more rapidly at first from a high of

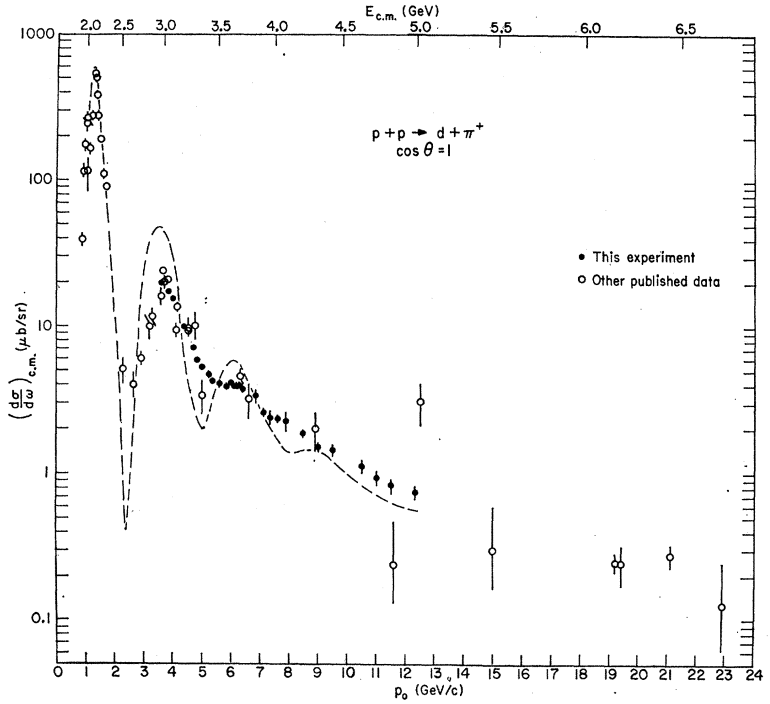

FIG. 13. Forward ($\cos\theta_{\text{c.m.}}=1$) differential cross section for the reaction $p+p\to d+\pi^+$ in the c.m. system as a function of incident proton laboratory momentum p_0 and total energy in the c.m. system $E_{\text{c.m.}}$, including previously published work (Refs. 7–11 and 20–26). All data shown were either measured directly at $\cos\theta_{\text{c.m.}}=1$, extrapolated to $\cos\theta_{\text{c.m.}}=1$ from a measured angular distribution of the form $a+b\cos^2\theta_{\text{c.m.}}$, or extrapolated to $\cos\theta_{\text{c.m.}}=1$ using the relation $e^{-p_\perp/b}$, where $p_\perp$ is the transverse momentum in GeV/c and b varies between 0.26 and 0.19 GeV/c (see Ref. 23). The curve is from a calculation of the one-pion-exchange contribution according to the model of Yao (Ref. 28).

15.0 μb/sr at 3.4 GeV/c, flatten off at 2.5 μb/sr around 6.0 GeV/c, and then decrease rather regularly for higher values of incident momentum. At our highest momentum, 12.3 GeV/c, the cross section has fallen to 0.44 μb/sr. In contrast, the elastic channel in pp collisions has differential cross sections in the forward direction which increase over the range of incident momenta covered here. At 12.3 GeV/c, the pp elastic scattering cross section in the forward direction is more than 10^5 times greater than in the $d\pi^+$ channel.

In the last column of Table I we have attempted to extrapolate the cross sections obtained very near the forward direction to exactly 0°. In carrying out this program, we made use of the relation

$$(d\sigma/d\omega)_{\text{c.m.}}=(d\sigma/d\omega)_0 e^{-p_\perp/b} \tag{4}$$

found by Allaby *et al.*[19] to give a good fit to the data at 21.1 GeV/c and at 3.62 GeV/c. Here $p_\perp$ is the transverse momentum in GeV/c. The parameter b seems to be somewhat energy dependent. According to Allaby, it is equal to 0.26 GeV/c for the data of Heinz *et al.*[9] at $E_{\text{c.m.}}=3.0$ GeV and to 0.19 GeV/c for their own data at $E_{\text{c.m.}}=6.4$ GeV. In the absence of more precise information, we used values of b varying linearly with $E_{\text{c.m.}}$ between these two values.

The over-all behavior of the cross section becomes more apparent when our data are combined with other measurements as listed in Table II. In Fig. 13 we have plotted all available c.m. differential cross sections for the reaction $p+p\to d+\pi^+$ at 0°, for $E_{\text{c.m.}}>2.3$ GeV either as measured directly or extrapolated using Eq. (4). Three features are evident. The first is a well-known peak at $p_0=1.25$ GeV/c ($E_{\text{c.m.}}=2.17$ GeV). There is a second pronounced maximum at $p_0=3.5$ GeV/c ($E_{\text{c.m.}}=3.0$ GeV). Finally, there is a definite shoulder centered at $p_0\approx 6.3$ GeV/c ($E_{\text{c.m.}}=3.7$ GeV). Beyond this energy further structure is not evident. The cross section decreases rather smoothly up to $p_0=22.9$ GeV/c ($E_{\text{c.m.}}=6.7$ GeV/c), the highest energy measured to date.[23] In the region $2.3<E_{\text{c.m.}}<3.0$ GeV, the angular distribution, as measured both by Dekkers *et al.*[8] (who measured the inverse reaction) and by Heinz *et al.*,[9] is changing very rapidly near 0°, making the extrapolation rather uncertain. Therefore, in this energy interval the data of Dekkers, Heinz, and one

[19] J. V. Allaby, F. Binon, A. N. Diddens, P. Duteil, A. Klovning, R. Meunier, J. P. Peigneux, E. J. Sacharidis, K. Schlüpmann, M. Spighel, J. P. Stroot, A. M. Thorndike, and A. M. Wetherell, Phys. Letters **29B**, 198 (1969).

[20] N. W. Reay, A. C. Melissinos, J. T. Reed, T. Yamanouchi, and L. C. L. Yuan, Phys. Rev. **142**, 918 (1966).

[21] M. A. Abolins, R. Graven, R. McCarthy, G. A. Smith, L. H. Smith, A. B. Wicklund, R. L. Lander, and D. E. Pellett, Phys. Rev. Letters **25**, 469 (1970).

[22] K. Ruddick, L. G. Ratner, K. W. Edwards, C. W. Akerlof, R. H. Hieber, and A. D. Krisch, Phys. Rev. **165**, 1442 (1968).

[23] W. F. Baker, E. W. Jenkins, A. L. Read, A. D. Krisch, J. Orear, R. Rubinstein, D. B. Scarl, and B. T. Ulrich, Phys. Rev. **136**, B779 (1964).

[24] R. C. Lamb, R. A. Lundy, T. B. Novey, D. D. Yovanovitch, and R. Lander, Phys. Rev. Letters **17**, 100 (1966).

[25] R. Durbin, H. Loar, and J. Steinberger, Phys. Rev. **84**, 581 (1951); T. H. Fields, J. G. Fox, J. A. Kane, R. A. Stallwood, and R. B. Sutton, *ibid.* **95**, 638 (1954); H. I. Stadler, *ibid.* **96**, 496 (1954); C. E. Cohn, *ibid.* **105**, 1582 (1957); M. G. Mescheryakov, B. S. Neganov, N. P. Bogachev, and V. M. Sidorov, Dokl. Akad. Nauk SSSR **100**, 673 (1955); M. G. Mescheryakov and B. S. Neganov, *ibid.* **100**, 677 (1955); B. S. Neganov and L. B. Parfenov, Zh. Eksperim. i Teor. Fiz. **34**, 767 (1958) [Soviet Phys. JETP **7**, 528 (1958)].

TABLE II. Measurements of deuteron production in the reaction $p+p \rightarrow d+\pi^+$ for total c.m. energy above 2.3 GeV.

Reference	θ[a]	$E_{c.m.}$[b] (GeV)
7	90–156°	2.3
9	90–165°	2.3–3.0
8[c]	90–172°	2.5–3.3
20	180°	2.8
10	180°	2.5–2.9
This work[d]	87 mrad	2.9–5.0
11[e]	60 mrad	3.0–4.3
21	180°	3.0, 3.2
22	90°	3.4
23	56°	4.9
	43°	5.5
	35°	6.7
24	0°	5.0
19[e]	40 mrad	6.15
	25 mrad	6.2
	12–60 mrad	6.4

[a] Angle of emission of the deuteron with respect to the incident proton direction. Angles expressed in degrees are in the c.m. system. Angles expressed in mrad are in the laboratory system.
[b] Total c.m. energy.
[c] Measured the inverse reaction $\pi^+ + d \rightarrow p+p$.
[d] Detected the deuterons emitted backward in the c.m. system.
[e] Detected the deuterons emitted forward in the c.m. system.

point from the present work have not been shown. For $E_{c.m.} \gtrsim 3.0$ GeV, Eq. (4) was assumed to hold. Also shown are sufficient data[25] below $E_{c.m.}=2.3$ GeV to indicate the peak at $E_{c.m.}=2.17$ GeV. In this region the angular distribution of reaction (1) (and its inverse) has a simple $a+b\cos^2\theta_{c.m.}$ angular dependence, so that the extrapolation to 0° could be made reliably. It is interesting to note that with the above deletions, all data in the region $2.3<E_{c.m.}<6.7$ GeV appear to be consistent. Even the very high transverse momentum data of Baker *et al.*[23] and Ruddick *et al.*[22] seem to fall on a smooth curve once the extrapolation to 0° is carried out according to Eq. (4). The one point of Lamb *et al.*[24] at $E_{c.m.}=5.0$ GeV is in marked disagreement with what otherwise is a consistent set of points. Lamb *et al.*[24] identified reaction (1) by measuring the momentum of pions emitted at 180° and requiring the MM to be that of the deuteron. We have no ready explanation why this type of measurement should appear to overestimate the cross section by such a large factor. We have deleted this point in the analysis that follows.

We found that it was possible to fit the differential cross sections for reaction (1) by modifying the empirical formula introduced by Orear[26] as follows:

$$(d\sigma/d\omega)_{c.m.}=A\,(s/s_0)^a e^{-p_\perp/b}\,, \tag{5}$$

where $s_0=1$ GeV^2, s is the total c.m. energy squared in GeV^2, and $p_\perp$ is the transverse momentum in GeV/c. Orear[26] took $a=-1$ and determined $A=0.12$ mb/sr and $b=0.16$ GeV/c. This relation gave a reasonable fit to the data at high energy and high transverse momentum, but it failed to predict the correct behavior of the differential cross section at high energy and low momentum transfer. At $E_{c.m.}=5$ GeV it gives a forward differential cross section which is too large by more than a factor of 6. Using all the available data for $E_{c.m.}>3.9$ GeV, we determined the parameters in Eq. (5) and obtained

$$A=2.60\pm0.71 \text{ mb/sr}\,,$$
$$a=-2.5\pm0.1\,,\quad b=0.20\pm0.01 \text{ GeV}/c\,.$$

The fit, which includes 23 data points, has a χ^2 per degree of freedom of 0.8. These data have been plotted in Fig. 14 to show the s dependence of the cross section in the high-energy region. The forward differential cross section is seen to fall off like $s^{-2.5}$.

The appearance of three peaks at $E_{c.m.}=2.17$, 3.0, and 3.7 GeV suggests a connection with the first three resonances in π^+p elastic scattering, namely, the first three $T=\frac{3}{2}$ nucleon isobars at $M_\Delta=1.236$, 1.950, and 2.420 GeV. The connection was first pointed out by Chahoud, Russo, and Selleri[27] following the discovery of the second peak in reaction (1) by Cocconi *et al.*[11] This follows easily from the OPE model [Fig. 15(a)] and is due to the fact that the binding of n and p into a deuteron fixes the kinematics of the three-body intermediate state with the following relationship:

$$s'=\tfrac{1}{2}(s-M^2+\mu^2)+m^2\,, \tag{6}$$

where s is the square of the total c.m. energy for reaction (1), $s'=M_\Delta{}^2$ is the invariant mass of the πN system, and M, m, and μ are the deuteron, nucleon, and pion masses, respectively. This formula neglects the deuteron binding energy and the momentum distribution of the bound nucleons, but these can be shown to have only a minor effect on the validity of Eq. (6). Equation (6) predicts peaks at $E_{c.m.}=2.19$, 3.06, and 3.67 GeV, in close correspondence with the observed maxima. No other peaks appear, which is a consequence of the isospin structure of the OPE diagram.[27] This predicts that other peaks such as those corresponding to the $T=\frac{1}{2}$ isobars, would be suppressed by a factor of 16 compared to the $T=\frac{3}{2}$ isobars.

These aspects and the success of the OPE model in the interpretation of pion production in pp collisions in the 1–2-GeV region led Yao[28] to attempt a more complete calculation of the $d\pi^+$ production. In Yac's formulation the matrix elements which appear in the calculation are evaluated in terms of the $\pi^\pm p$ elastic and charge-exchange scattering cross sections in the following form:

$$\frac{d\sigma}{d\omega}(s,\theta)=G(s,\theta)\left(3\frac{d\sigma^+}{d\omega_\pi}-\frac{d\sigma^-}{d\omega_\pi}+3\frac{d\sigma^0}{d\omega_\pi}\right)+(p_1\rightleftarrows p_1')\,. \tag{7}$$

Here, $G(s,\theta)$ is a slowly varying function of the square

[26] J. Orear, Phys. Letters **13**, 190 (1964).

[27] J. Chahoud, G. Russo, and F. Selleri, Phys. Rev. Letters 11 506 (1963).

[28] T. Yao, Phys. Rev. **134**, B454 (1964). According to M. E. Schillaci and R. R. Silbar [Phys. Rev. **171**, 1764 (1968)], a factor $\approx 1/0.6$ was neglected by Yao in his final result. Our calculation does not include this factor.

of the total c.m. energy s, θ is the angle between the incoming proton and the outgoing deuteron in the c.m. system, $0 \leqslant \theta \leqslant \frac{1}{2}\pi$, and $d\sigma/d\omega_\pi$ are the differential πp scattering cross sections, evaluated at their total c.m. energy squared s' (Eq. 6) and their c.m. scattering angle θ'.

The function $G(s,\theta)$ was determined entirely from other experiments and contains such factors as the pion-nucleon coupling constant $G^2/4\pi$, the deuteron form factor, as well as the Ferrari-Selleri off-the-mass-shell correction function as given in Yao's paper.[28]

The second term in Eq. (7) is obtained from the first term by interchanging p_1 and p_1' [see Fig. 15(a)]. This interchange amounts to changing $\cos\theta$ to $-\cos\theta$. The four-momentum squared k_1^2 of the exchanged virtual pion is given by

$$-k_1^2 = -2m^2 + \tfrac{1}{4}(s + M^2 - \mu^2) - qp\cos\theta\,, \qquad (8)$$

where p and q are the three-momenta in the c.m. system of the incoming proton and outgoing deuteron, respectively, θ is as defined in Eq. (7), and s, M, m, and μ are as defined in Eq. (6). For $\cos\theta = 1$, $\cos\theta' = -1$ and $-k_1^2$ is a minimum. From this it follows that backward πp scattering is very important for deuteron formation in the forward direction. It is by backward emission of the π^+ at the upper vertex [see Fig. 15(a)] that the nucleon momentum may be reversed in direction and made equal to that of the nucleon emerging from the lower vertex after emitting a pion with small k_1. The factor $G(s,\theta)$ is a maximum in this case.

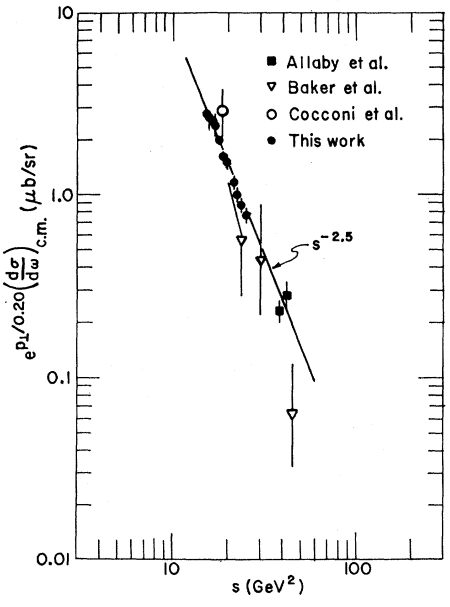

FIG. 14. Differential cross section for the reaction $p+p \to d+\pi^+$ in the c.m. system. The function $e^{p_L/b}(d\sigma/d\omega)_{\text{c.m.}}$ is plotted against the total energy squared in the c.m. system ($s = E_{\text{c.m.}}^2$) for $E_{\text{c.m.}} > 3.9$ GeV, including previously published work (Refs. 11, 23, 24). The curve shown is the result of fitting the experimental data with a function of the form $A\,(s/s_0)^a e^{-p_L/b}$.

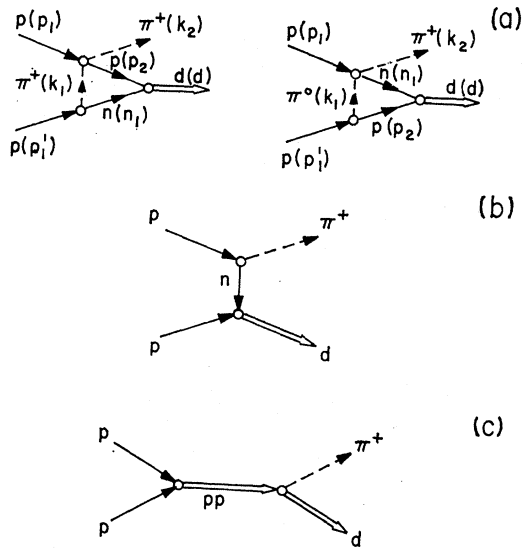

FIG. 15. Feynman diagrams for the reaction $p+p \to d+\pi^+$ proceeding via (a) one-pion-exchange with the exchange of either a π^+ or a π^0 meson, (b) one-nucleon-exchange, and (c) the formation of a dibaryon resonance in the direct channel.

The contribution of the second term corresponds to $\cos\theta = -1$, $\cos\theta' = 1$. In this case $-k_1^2$ is very large, the exchanged virtual pion is very far from the mass shell, and the OPE approximation becomes highly dubious. The value of $G(s,\theta)$ itself will be small, but since forward πp scattering cross sections are quite large, the second term can make an appreciable, albeit questionable, contribution.

The curve given in Fig. 13 was calculated using Eq. (7) and the data for πp scattering taken from the open literature and, in particular, from the recent compilation of Giacomelli, Pini, and Stagni.[29] The data corresponding to forward and backward πp scattering used in our calculation are shown in Figs. 16 and 17. Such a calculation neglects the interference between the two contributions, corresponding to the incoherent sum. The interference effect can be quite large, enough to alter the cross section by a decade of more.

The results of the Yao calculation neglecting interference appear to give a reasonably good account of the experimental data, and most of the experimental points fall within the range of values permitted by including interference effects. Although the bounds are wide, we must consider that the agreement is remarkably good considering that all the available parameters in Yao's expression for the cross section (except for the relative phase of the amplitudes) have been determined from other experiments. In particular, the agreement emphasizes the role played by the direct-channel, $T = \frac{3}{2}$, Δ resonances in the πp system.

The OPE model is only one of several different models that have been used in the interpretation of the process

[29] G. Giacomelli, P. Pini, and S. Stagni, CERN/HERA Report No. 69-1 (unpublished).

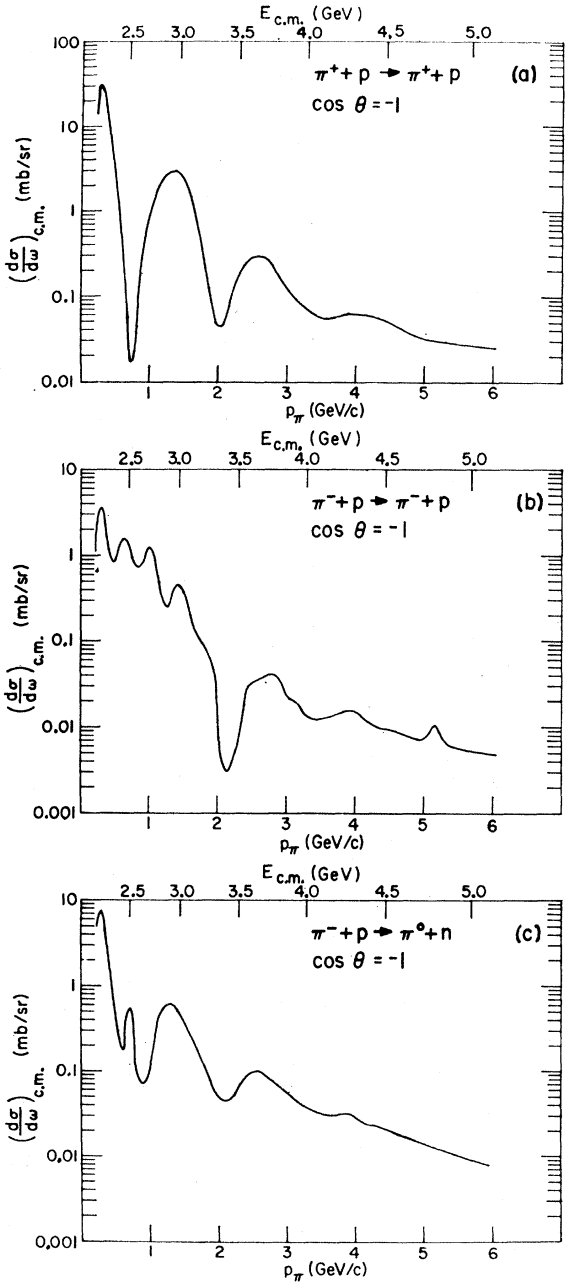

FIG. 16. Backward differential cross section in the c.m. system for (a) π^+p elastic scattering, (b) π^-p elastic scattering, and (c) π^-p charge exchange scattering as a function of incident pion laboratory momentum p_π. It should be noted that the variable $E_{\text{c.m.}}$ does not refer to the total energy in the c.m. system of the πp but to the total energy in the c.m. system of the reaction $p+p \rightarrow d+\pi^+$. The two systems have been related through the kinematics as given by the Yao model as discussed in the text. The data are from a survey of the literature (see Ref. 30). The curves are hand fits to the data.

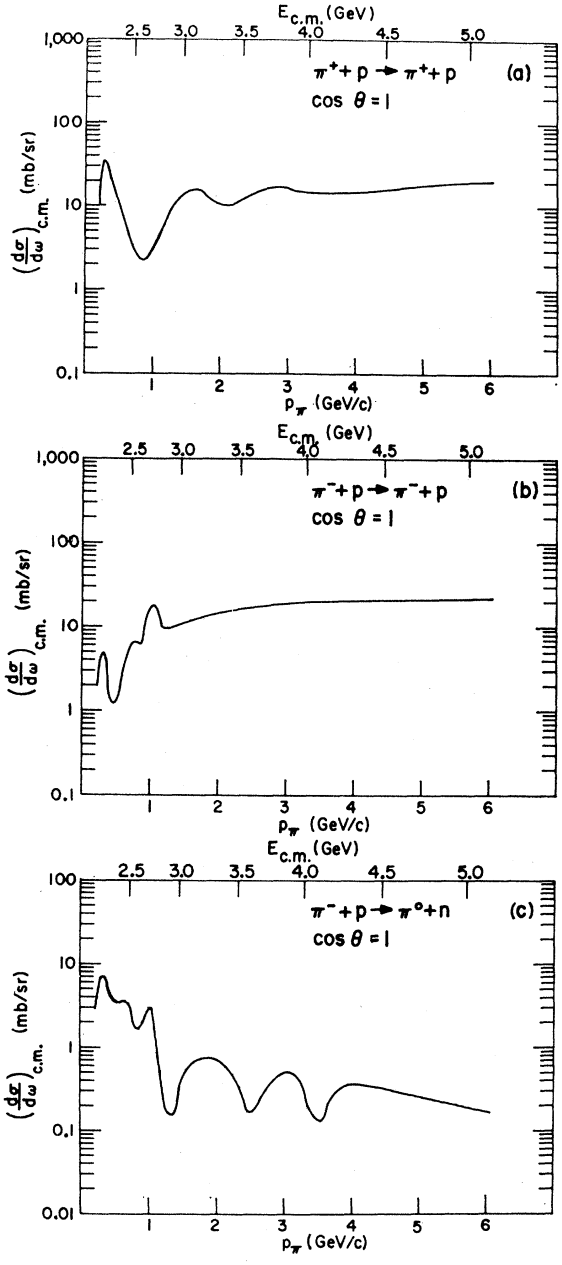

FIG. 17. Forward differential cross section in the c.m. system for (a) π^+p elastic scattering, (b) π^-p elastic scattering, and (c) π^-p charge exchange scattering as a function of incident pion laboratory momentum p_π. See the caption for Fig. 16 for additional details.

under consideration here. We have already alluded to the ONE model in connection with the work of Heinz *et al.*[9] This has been reviewed by Brown.[30] The graph for this is given in Fig. 15(b). Such a graph can give no resonant structure because there are no poles occurring in the propagator in the physical region. According to Brown[30] the ONE graph gives a smooth behavior, much too large a cross section, and too slow a falloff with energy. At 12 GeV/c the prediction is some 20 times larger than the experimental value. However, a part of the reaction amplitude must be due to such a graph. How to understand what inhibitions operate

[30] D. J. Brown, Nucl. Phys. **B7**, 37 (1968).

to reduce its contribution to the muchsmaller level that it evidently obtains is the question.

This question has been reconsidered by Uchiyama-Campbell and Silbar,[31] who point out that the *dnp* vertex involves an exchanged neutron leg which is rather far off shell. For the measurements under consideration here, the momentum transfer u between the incoming proton and outgoing pion varies from about 0.3 $(\mathrm{GeV}/c)^2$ down toward 0. Not much is known about the value of the vertex function for such small values of u. In view of this, a strong momentum dependence of the vertex function could drastically reduce the contribution of this graph. Moreover, absorption effects in the initial and final states can produce a further reduction. An attempt to impose absorption effects on the helicity amplitudes was carried out[31] and a significant reduction in the predicted cross sections was obtained. However, the result was still larger than the experiment, presumably because of the dubious treatment of the *dnp* vertex.

One problem with the ONE graph is that it gives the wrong energy dependence. An improvement could be anticipated by Reggeizing the exchanged nucleon. A detailed discussion of the Reggeization in this case has been given by Lee.[32] Unfortunately, with Regge models usable formulas are obtained only in the asymptotic high-energy limit. Here the theory gives an amplitude proportional to

$$\frac{1}{\Gamma(\alpha+\frac{1}{2})}\left[\frac{1\pm e^{-i\pi(\alpha-1/2)}}{\cos\pi\alpha}\right]s^{\alpha-1/2}, \tag{9}$$

where $\pm$ is taken according to the signature of the trajectory. This leads to a differential cross section

$$d\sigma/du\sim s^{2\alpha(u)-2}. \tag{10}$$

For a one-Regge-pole model with exchange by the $N_\alpha(\frac{1}{2}^+(0.938), \frac{5}{2}^+(1.688), \ldots)$ trajectory, the usual assumption of linear dependence gives $\alpha=-0.38+1.0u$, so that for zero u the exponent of s is -2.76.

However, Barger and Michael[33] have pointed out that for this trajectory alone the amplitude has a zero at $\alpha=-\frac{1}{2}$, or at $u=-0.12$ $(\mathrm{GeV}/c)^2$, well within the physical region. The experimental data of Allaby *et al.*[19] at 21.1 GeV/c shows no such pronounced dip. This fact is taken as evidence for the contribution of another trajectory of opposite signature, namely, $N_\gamma(\frac{3}{2}^-(1.518), \frac{7}{2}^-(2.190), \ldots)$ with $\alpha=-0.8+1.0u$. Thus, the total amplitude should be a sum of two terms with zeros that do not coincide. In Regge language this situation is referred to as exchange degeneracy.[33] As noted by Barger and Michael, the exchange-degenerate model is somewhat of an idealization since the N_α and N_γ trajectories are split apart. They constructed an "effective" trajectory between the two

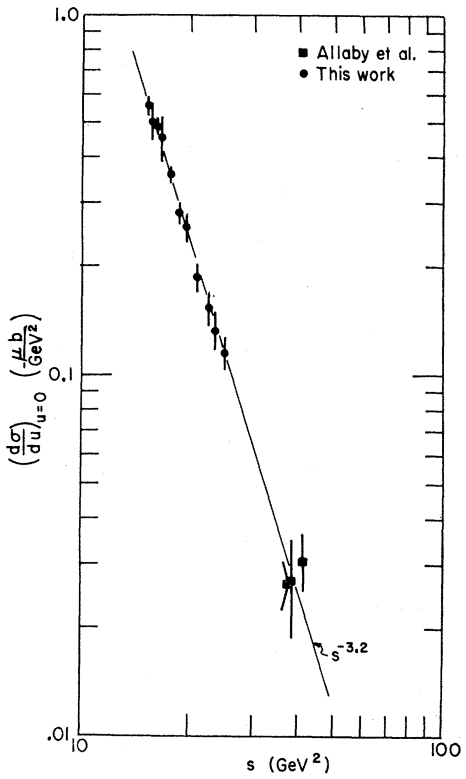

FIG. 18. Plot of $(d\sigma/du)$ at $u=0$ to show the s dependence above 7.1 GeV/c. The experimental data have been extrapolated to $u=0$ using the factor $\exp(-p_\perp/0.20)$ as discussed in the text. The points near $s=40$ GeV^2 are from Ref. 23.

wrong-signature nonsense points $\alpha(N_\alpha)=-\frac{1}{2}$ and $\alpha(N_\gamma)=-\frac{3}{2}$ obtaining $\alpha_{\mathrm{eff}}=-0.9+0.28u$. This effective trajectory yields a differential cross section for zero u with the exponent of s equal to -3.8.

To obtain a rough estimate of the experimental behavior, we used the factor $\exp(-p_\perp/0.20)$ to extrapolate our differential cross sections above $E_{\mathrm{c.m.}}=3.9$ GeV and those of Allaby *et al.*[19] to give $d\sigma/du$ at $u=0$. Such a procedure has questionable validity but we have, nevertheless, plotted the result in Fig. 18 together with a least-squares fit to the data. The fit yields an exponent of s equal to -3.2, a result between the values set by considering a single N_α trajectory or an effective trajectory.

Barger and Michael[33] also considered the full kinematics[32] for Reggeization of reaction (1), using both N_α and N_γ trajectories and certain simplifying assumptions. By parametrizing the residues of the helicity amplitudes, they obtained a good fit to the high-energy portion of the forward cross section, as well as the 21.1-GeV/c angular distribution. However, these results required four otherwise undetermined parameters.

The inadequacy of a simple Regge pole model to fit our data has also been recognized by Brown[34] who

[31] F. Uchiyama-Campbell and R. R. Silbar, LASL Report No. LA-DC-10315, 1969 (unpublished).
[32] H. Lee, Phys. Rev. **174**, 2130 (1968).
[33] V. Barger and C. Michael, Phys. Rev. Letters **22**, 1330 (1969).
[34] D. J. Brown, Can. J. Phys. **47**, 2001 (1969).

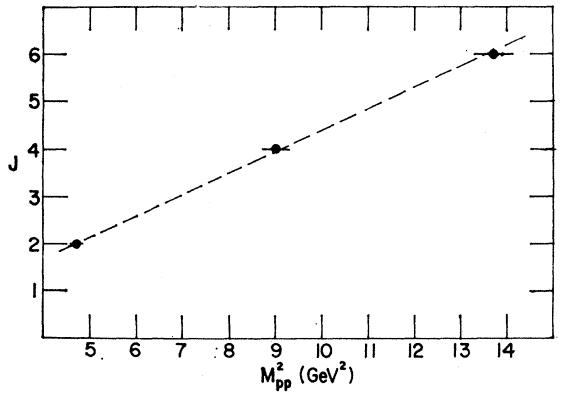

FIG. 19. Total c.m. energy squared of the pp system ($s=M_{pp}^2$) versus the integer J suggesting a Regge trajectory for the dibaryon system. The data are taken from the features appearing in the forward differential cross section for the reaction $p+p\rightarrow d+\pi^+$.

showed that a good fit could be obtained if the process is dominated by a Regge cut.

It is interesting to suggest that the three bumps in the forward cross section are due to direct-channel dibaryon resonances according to the graph of Fig. 15(c). These fall on a linear rising trajectory as shown in Fig. 19. The linear behavior follows from Eq. (8) which shows that if $M_\Delta^2=s'$ has a linear behavior, then $M_{pp}^2=s$ will have one as well.

According to Graffi, Grecchi, and Turchetti,[35] the first peak may be the first Regge recurrence of the $^1S_0$ pp pole (the unbound diproton) and arise from a $^1D_2$ resonance in the pp system. Evidence for such a resonance has been given by Arndt[36] based on a partial-wave analysis of the elastic pp scattering around 660 MeV.

However, the $^1D_2$ phase shifts are not very large and the argument that a pole exists in a nonphysical region must be considered speculative at this stage. On the other hand, Mandelstam[5] has argued that the strong resonant behavior of the $d\pi^+$ channel in this energy region could be explained in terms of an s-wave $\Delta_{3/2,3/2}p$ resonance with the same quantum numbers as $^1D_2$. Following this idea, the other bumps in our curve would correspond to further Regge recurrences at $M_{pp}=3.0$ and 3.7 GeV with $J=4$ and $J=6$, respectively. A partial-wave analysis based on careful measurements of the angular distribution in the energy region of the bumps might help decide the angular momentum character and parity of these states.

Other evidence for the existence of such a dibaryon trajectory has been reviewed by Libby and Predazzi[37] and supports the plausibility of this idea, but emphasizes the lack of good and convincing data.

The suggestion of dibaryon resonances is, of course, just one aspect of the larger subject of "exotic" resonances for which there is presently little evidence. However, if a duality principle[13] applies here, we should expect that s-channel low-energy resonances would follow naturally as an alternative description of the process of t- and u-channel Regge exchange.

In conclusion, this discussion brings out the primitive and ambiguous state of the theory of strong-interaction processes. Surprisingly, in spite of its known inadequacies, especially in the description of high-energy processes and those involving high momentum transfers, the OPE mechanism offers the most satisfactory description of our data. The implication is that we are still far from the asymptotic limit for which simple Regge ideas can be expected to dominate.

ACKNOWLEDGMENTS

It is a pleasure to acknowledge the contributions of R. L. Armstrong, G. Black, R. R. Gabriel, C. L. Hung, J. P. Legault, J. W. Lillberg, J. G. Michelassi, P. A. Plowe, J. Redfern, R. A. Ryan, and R. B. Wilberg in the construction of the apparatus and the running of the experiment, and the help of V. Stovall and A. LaRotonda in the data reduction. We wish to thank Dr. G. J. Igo and Dr. K. W. Edwards for their help in some stages of the experiment. Dr. R. R. Silbar helped us anticipate what results we might expect. Dr. E. P. Steinberg gave us important advice about the measurement of the beam intensity and put his equipment for this purpose at our disposal. One of us (E. P. H.) wishes to thank Professor R. D. Barton for helpful discussions regarding the time-of-flight instrumentation. In addition, H. L. A. wishes to thank Professor G. Wentzel, Professor Y. Nambu, and Professor M. K. Sundaresan for useful discussions of the results. We appreciated the hospitality of the Argonne National Laboratory and the help of various members of the Argonne ZGS staff. In particular, C. W. Testin gave invaluable assistance with the alignment of our spark chambers, A. R. Passi helped with the installation of our equipment on the ZGS floor, and R. J. Lari measured the effective length of the bending magnets. Other members of the ZGS staff contributed in the competent operation of the accelerator and auxiliary equipment.

[35] S. Graffi, V. Grecchi, and G. Turchetti, Nuovo Cimento Letters 2, 311 (1969).
[36] R. A. Arndt, Phys. Rev. 165, 1834 (1968).
[37] L. M. Libby and E. Predazzi, Nuovo Cimento Letters 2, 881 (1969).